# Copyright Warning & Restrictions

The copyright law of the United States (Title 17, United States Code) governs the making of photocopies or other reproductions of copyrighted material.

Under certain conditions specified in the law, libraries and archives are authorized to furnish a photocopy or other reproduction. One of these specified conditions is that the photocopy or reproduction is not to be "used for any purpose other than private study, scholarship, or research." If a, user makes a request for, or later uses, a photocopy or reproduction for purposes in excess of "fair use" that user may be liable for copyright infringement,

This institution reserves the right to refuse to accept a copying order if, in its judgment, fulfillment of the order would involve violation of copyright law.

Please Note: The author retains the copyright while the New Jersey Institute of Technology reserves the right to distribute this thesis or dissertation

Printing note: If you do not wish to print this page, then select "Pages from: first page # to: last page #" on the print dialog screen

# ABSTRACT

## DEVELOPMENT OF A FIBER OPTIC POLARIMETRIC SENSOR FOR CONCRETE

by
Insang Lee

Development of a fiber optic sensor for embedment in cementitious composites and measurement of displacements associated with the opening of microcracks is described. The sensor can be employed as a transducer for measurement of crack tip opening displacements during fracture tests. A polarization maintaining fiber is used as the sensing element, and transduction mechanism is similar to those of other polarimetric type based sensors. However, the deformation resolving power of the sensor is increased by way of increasing the effective length of the optical fiber. This is done by winding the optical fiber into a coil. A direct relationship between the number of loops in the coil and sensitivity of measurements is obtained. A calibration procedure is developed by which the optical signal is converted to displacements. The sensor was employed in a series of fracture tests. Experiments involved embedment of the optical fiber in concrete beams. Specimens were center edge notched, and the fiber coil sensors were embedded at the tip of the notch. This arrangement allowed for direct measurement of displacements associated with the opening of microcracks at the crack tip. Experimental results are presented, and crack tip opening displacement(CTOD) results are compared with crack opening displacements(COD) measured by conventional transducers at the crack mouth.

# DEVELOPMENT OF A FIBER OPTIC POLARIMETRIC SENSOR FOR CONCRETE

by
Insang Lee

A Thesis
Submitted to the Faculty of
New Jersey Institute of Technology
in Partial Fulfillment of the Requirement for the degree of
Master of Science in Civil Engineering

Department of Civil and Environmental Engineering

May 1996

## APPROVAL PAGE

## DEVELOPMENT OF A FIBER OPTIC POLARIMETRIC SENSOR FOR CONCRETE

**Insang Lee**

Dr. Farhad Ansari, Thesis Advisor — Date
Professor of Civil and Environmental Engineering, NJIT

---

Prof. Edward G. Dauenheimer, Committee Member — Date
Professor of Civil and Environmental Engineering, Associate Chairman and Graduate Advisor, NJIT

---

Dr. George Pincus, Committee Member — Date
Distinguished Professor of Civil and Environmental Engineering, NJIT

## BIOGRAPHICAL SKETCH

**Author:** Insang Lee

**Degree:** Master of Science

**Date:** May 1996

**Undergraduate and Graduate Education:**

- Master of Science in Civil Engineering,
  New Jersey Institute of Technology, Newark, NJ, 1996

- Bachelor of Engineering in Civil Engineering,
  Korea University, Seoul, Korea,1992

**Major:** Civil Engineering

To my beloved father and mother

# ACKNOWLEDGMENT

I would like to express my deepest appreciation to my thesis advisor, Professor Farhad Ansari, for his guidance, support, and encouragement throughout this research.

Special thanks to Professors Edward G. Dauenheimer and George Pincus for serving as members of the committee.

I appreciate the timely help and expert assistance from the Smart Structure Laboratory members, including: Libo Yuan, Xi Chen, Hong Ding, Guanyong Zhang, and Ping Jiang.

And finally, I thank Allyn Luke for his assistance on the experiment.

## TABLE OF CONTENTS

## LIST OF FIGURES

# CHAPTER 1

# INTRODUCTION

## 1.1 Introduction

Cracking is among the important parameters that directly influence the structural design and durability of structure. Many fracture mechanics models have been proposed in recent years to account for the nonlinear behavior of concrete elements[1]. Nonlinear characteristics of fracture in concrete are associated with the microcracking zone (process zone) in front of the crack tip[2].

Most fracture models represent the fracture process zone with a damage band or a band of crack closing pressure which depends on the crack opening displacement, i.e. the post-peak stress-displacement relationship. The accuracy of these models relies significantly on the selected post-peak stress-displacement relationship. One parameter of significant importance in determining fracture properties is crack tip opening displacement (CTOD). For instance, crack extension or fracture may be assumed to occur when the crack opening displacement exceeds a critical value.

To date, experimental determination of CTOD has been an impossibility. For these reasons researchers have resorted to measurement of crack mouth opening displacement (COD) on a notched or precracked specimen by linear variable displacement transducers (LVDT) or clip gauge extensometers. It is logical to assume that the crack mouth opening displacements measured in this way should be larger than the real displacements at the crack tip. This is due to the fact that in comparison with CTOD,

COD represents displacements at distances further away from the neutral axis of the beam. Furthermore, COD values are more representative of global displacements rather than deformations specific to the formation of process zone in cementitious composites. For these reasons, attempts have been made to determine CTOD from measurement of surface deformations using laser speckle interferometry[3].

These studies indicated the localized nature of microcracking at the crack tip, and the need for characterization of displacements in terms of the opening of microcracks within the process zone. Therefore, the sensor developed in the present study offers sufficient sensitivity for this purpose.

## 1.2 Objective

The objective of the research presented here is to develop, calibrate and test an embedded optical fiber CTOD sensor for applications in fracture mechanics studies of cementitious composites. Among the important characteristics of optical fibers are small size, geometric adaptability, and the ability to act as the sensor as well as the signal path. These are important attributes, especially in considerations for design of practicable embedded sensors in concrete and other cementitious composites.

In general, fiber optic sensors are categorized into various types depending on the application and transduction mechanism employed for discernment of material deformations. A brief discussion pertaining to various types of fiber optic sensors will be given in the background section of this thesis. It is important to note that development of a suitable CTOD sensor for concrete requires sufficient sensitivity for measurement of

deformations, economy in terms of sensor complexity, instrumentation, and practicality and ease of installation during placement of fresh concrete. The sensor described herein was designed based on the above-mentioned considerations. A calibration technique is developed for conversion of optical signals to corresponding displacements. The capability of the fiber optic sensor in terms of sensitivity and resolution power for measurement of CTOD is demonstrated through experiments with single edge notched concrete beams under three point bending conditions.

## 1.3 Background

Transmission of light through optical fibers can be explained by the Snell's law and the concept of total internal reflection[4]. According to Figure 1.1, as indicated by the refractive index, n, when light travels from the fiber core that has a high refractive index into the cladding with a lower index, the lightwave totally reflects back to the core.

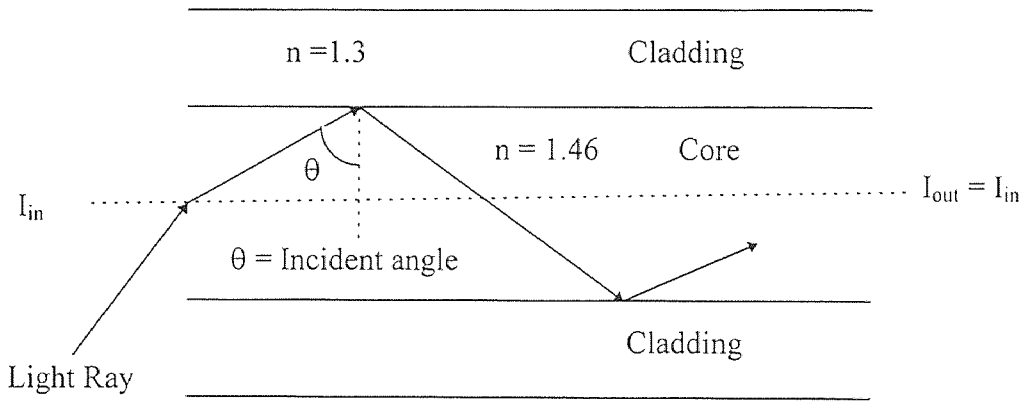


**Figure 1.1** Propagation of a light ray in an optical fiber.

Depending on the diameter, and the refractive indices of the core and cladding, optical fibers may either carry only one(single-mode), or many modes(multi-mode) of the lightwave. Typical single-mode fibers have a core, cladding, and protective jacket diameters of respectively 50, 125, and 250 microns. Multi-mode fibers require a larger core diameter for allowing the propagation of various modes through the length. The core, cladding, and jacket diameters in typical multi-mode fibers are 50, 125, 250 microns respectively. Multi-mode fibers are easier to work with due to larger core diameters for coupling the light into and out of them.

## 1.4 Fiber Optic Sensor Types

Fiber optic sensors have been classified in a number of different ways[5]. For instance, they can be categorized based on the application, or the transduction mechanism. These classifications are diagrammatically depicted in Figure 1.2.

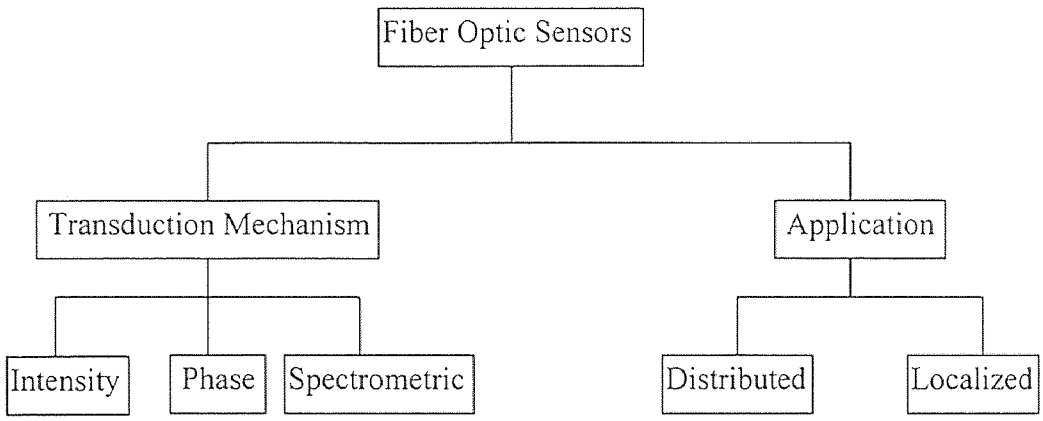


**Figure 1.2** Classification of fiber optic sensors.

Distributed sensors make full use of optical fibers, in that each element of the optical fiber is used for both measurement and data transmission purposes. A time of flight measurement along the optical fiber will determine locations and values of physical perturbations along the entire length of fiber. These sensors are most appropriate for large structure applications, due to their multi-point measurement capabilities. Localized fiber optic sensors determine the physical perturbation over a specific segment of the optical fiber, and are similar in that sense to conventional strain or temperature gauges.

Sensing based on intensity modulation pertains to light intensity losses that are associated with straining of optical fibers along any portion of their length. Sensors taking advantage of this phenomenon are termed as the intensity or amplitude type sensors. The advantage of intensity type sensors are the simplicity of construction, and the compatibility with multi-mode fiber technology.

Spectrometric sensors are widely employed in sensing of chemical reactions, and remote monitoring of contaminants in ground water. The transduction mechanism in these types of sensors is based on the changes in the wavelength of light to the physical perturbation of interest. An example of such sensors for measuring strains are Bragg grating type fibers (Morey et al. 1989). Introduction of Bragg gratings into fibers can be achieved by either external or internal manipulations. These sensors are intended for use only as a localized fiber optic sensor. The optical instrumentation for Bragg type sensors are highly intricate, as they require sensitive monochrometers for detecting the minute changes in the wavelength of light. However, they are highly sensitive, and very reliable for measurement of strain.

Phase sensors cover a broad range of optical phenomena for sensing purposes. A number of different configurations can be employed for measuring the change in the phase of light by an interferometric sensor. Interferometric sensors are highly sensitive for measuring strains. However, they require interference of light from two identically similar fibers, one of which is used as reference arm, for measuring the shifts in phase. An exception to a two arm interferometric sensor is a single fiber FabryPerot type sensor (Claus et al. 1993). In a FabryPerot type sensor, the fiber is manipulated in such a way so as to form two parallel partial mirrors, perpendicular to the axis of the fiber. The interference of the reflected signals which are formed in the cavity by the two partial mirrors create the interference pattern. FabryPerot sensor is only capable of providing localized measurements at the cavity formed by the two partial mirrors.

Another class of phase sensors take advantage of the polarization characteristics of light for transduction. These types of sensors are termed as polarimetric(Nanni et al.1991). Fringe shifts due to external perturbations in Polarization Maintaining(PM) fibers are caused by the interference of two mutually perpendicular polarized waves. The advantage in using a PM fiber for polarimetric transduction is that unlike their interferometric counterparts, only one fiber is needed for sensing the physical perturbation. Therefore, from practical application point of view, polarimetric sensors offer similar simplicities as the ones offered by the intensity sensors. Polarimetric sensors are much more sensitive than the intensity type. The sensitivity of polarimetric sensors is dependent on the polarization characteristics of the fiber, such as birefringent, and the beat length. Theoretically, polarimetric fiber sensors can be made as sensitive as the

interferometric types. However, the birefringence of the currently available PM fibers are not sufficient enough for optimum sensitivity.

### 1.5 Fiber Optic Sensors in Concrete

To date, only a limited number of studies report research activities pertaining to the application of fiber optic sensors in conjunction with testing or condition monitoring of concrete(Ansari et al.1991,92,93). The idea of using optical fibers for measuring temperature differentials due to exothermic processes in concrete has been already tested in Japan. Shimizu corporation employed fiber optic sensors for measurement of temperature differentials during construction of a tunnel(Photonics Spectra, 1990). In their application, a large number of sensors were employed in order to acquire temperature differentials throughout the tunnel. This was due to the effect that their sensors were of localized type, and each sensor was only able to achieve measurements at one single point. Their results had compared well with thermocouple measurements. Shimizu corporation's report indicated that the employment of localized sensor was not practical, and for practical applications in construction a distributed fiber optic sensor had to be developed.

Another type of sensor for studying the properties of concrete was developed by Ansari(1991). This sensor was employed for the detection of air bubbles and measurement of air content in fresh concrete during the construction. The sensor developed by Ansari was of intensity type, and the air bubble detection methodology was based on the sensor response to the refractive indices of air and concrete.

Rossi et al. (1989) employed an intensity type multi-mode fiber for detection of cracks in large concrete structures[6]. In his application, he had to remove the fiber coating in order for the crack opening displacements to produce sufficient effects in the fiber. The method was applied in monitoring the development of cracks at different locations within the shell of a motorway tunnel. The crack detection method was based on monitoring the drops in the intensity of the light output. The major disadvantage in using this technology was the extreme fragility of the uncoated optical fiber. Rossi's embedment technique involved protection of fibers by metallic tubes which were sequentially removed after pouring and casting operations. Shukla et al. (1993) employed MachZehnder(one kind of a phase sensor), and FabryPerot type sensors in the determination of stress intensity factors in single edge notch(SEN) laboratory specimens. Although, their work did not involve concrete, their results showed excellent correlation with theory.

Nanni et al.(1991) employed a polarimetric sensor for the measurement of compressive stresses and strains in concrete[7]. Nanni's work involved the use of a PM fiber which was embedded perpendicular to the direction of applied load. Their research results were especially interesting, since they considered the effect of interface shear transfer in between the fiber and the matrix for the interpretation of the optical signal. Sirkis et al.(1993) developed a general mechanism approach for the interpretation of the optical signal, and its relationship with interfacial strains. His work can be applied to concrete through proper modifications to his formulations.

Huston, Fuhr, and Ambrose(1993) developed a vibration detection technique by statistical manipulation of speckle patterns generated at the output end of the optical fiber.

In conjunction with condition monitoring of structures, they embedded fiber optic cables throughout a medical building facility in Burlington Vermont. Huston et al's report on intensity modulated sensors indicate that the intensity type sensors may not be sensitive enough for measurements of structural changes in concrete. Maher and Navy(1993) employed Bragg grating optical fiber(FOBG) sensors for the measurement of strain in large reinforced concrete beams. In their experiments, they attached the optical fiber to the reinforcement, and then embedded the reinforcement in a 10 by 12 inch, 10 ft long beam. Their research results indicated the FOBG sensors are extremely sensitive for the measurement of strains in reinforced concrete elements.

The European community has been more aggressive in the employment of fiber optic sensors in large scale structural monitoring operations[8,9]. For instance, Caussignac et al.(1992) has developed a load measuring sensor using multi-mode optical fiber. The optical fiber sensor is embedded inside elastomeric bearings fitted between the bridge deck and support. The light intensity loss is calibrated against the magnitude of the load. Holst and Habe(1992) developed an optomechanical arrangement for measuring the displacement of span joints in a concrete dam. Wolff and Miesseler(1992) employed intensity type sensors for monitoring deformations, and a number of chemical sensors for the detection of corrosion in Schiessbergstrasse prestressed concrete bridge.

# CHAPTER 2

# THEORETICAL BACKGROUND

## 2.1 Theory of the System

The sensor developed herein employs a high birefringent (Hi-Bi) optical fiber for sensing of strains and deformations. Hi-Bi fibers possess properties similar to those of birefringent materials employed in photoelasticity[10]. These fibers divide a circularly polarized light entering them into two modes along the two orthogonal axes (principal axes) of the optical fiber. Lightwave exiting the output of the fiber will also be circularly polarized (Figure 2.1).

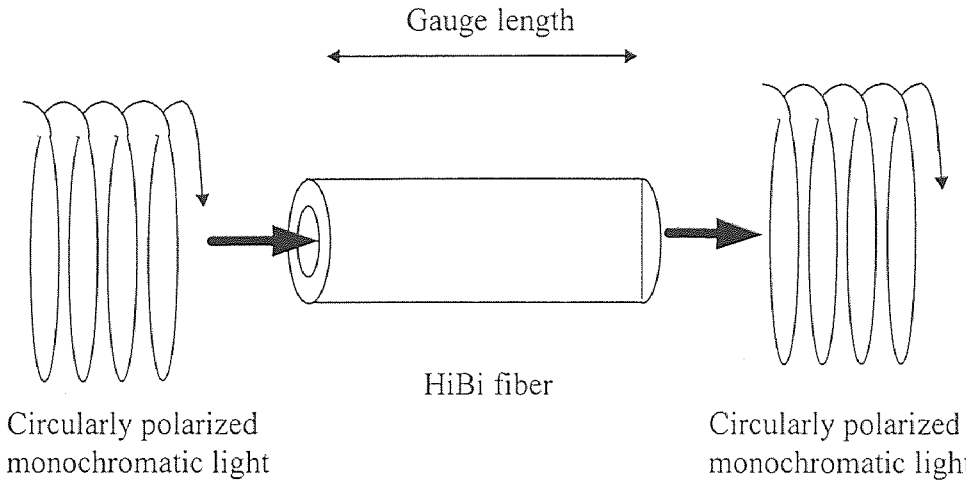


**Figure 2.1** Basic principle for a polarimetric sensor.

The intensity of light at the output end of the fiber is of the form[11, 12]

$$I = \frac{1}{2}(1 + \cos\phi) \tag{2.1}$$

where $I$ is the intensity of light in arbitrary unit, and $\phi$ is the relative phase retardation, and as it will be shown, it is related to the length, and optical properties of the fiber. In the absence of strains and/or other perturbations, the exiting light will have a constant output.

External perturbations such as deformations along the length of the optical fiber will cause interference of the two modes resulting in a change in the relative phase retardation by the amount $\Delta\phi$. The output intensity will have a sinusoidal shape, and in time domain, the period of this sinusoidal waveform is termed as a fringe. Frequency of the fringe pattern depends on the magnitude of the applied strain, and allows for development of a strain or deformation sensor through calibration. The relative phase retardation $\phi$ is related to the propagation constant, $\beta$, and the original length of the fiber, $l_0$ (gauge length), through the following relationship:

$$\phi = \beta l_0 \tag{2.2}$$

where $\beta = \frac{2\pi}{\lambda}(n_x - n_y)$ is the propagation constant, $\lambda$ is the wavelength of light propagating through the fiber, and $n_x, n_y$ are the refractive indices of the principal axes, respectively. Therefore, if $\Delta l_0$ is the elongation applied to the fiber, then the change in phase is

$$\Delta\phi = \beta\Delta l_0 + l_0\Delta\beta \tag{2.3}$$

where $\Delta\phi =$ phase change due to external perturbations.

The first term of Equation (2.3) represents the physical change of length produced by the strain. The second term, the change in $\phi$ due to a change in $\beta$, results from two effects: the strain-optics effect whereby the strain changes the refractive index of the fiber, and a

waveguide mode dispersion effect due to a change in fiber diameter, $a$, produced by longitudinal strain:

$$l_0\Delta\beta = l_0\left(\frac{d\beta}{dn}\right)\Delta n + l_0\left(\frac{d\beta}{da}\right)\Delta a \tag{2.4}$$

where $\beta = \left(\frac{2\pi}{\lambda}\right)\Delta n = \left(\frac{2\pi}{\lambda}\right)B$ , and $B = n_x - n_y$. The second term of Equation (2.4) can be dropped due to the fact that it is very small in comparison with the first term. This is due to the fact that the change in the diameter of the optical fiber will be very small, and therefore the change in $\beta$ with respect to $a$ is minute. Thus Equation (2.3) becomes:

$$\frac{\Delta\phi}{\Delta l_0} = \left(\frac{2\pi}{\lambda}\right)[B + l_0\left(\frac{\Delta B}{\Delta l_0}\right)] \tag{2.5}$$

Defining $T_\varepsilon$ as the amount of strain required to produce $2\pi$ phase shift (one fringe), and after omitting the intermediate steps, the change in phase due to strain can be expressed as:

$$\Delta\phi = \left(\frac{2\pi}{\lambda}\right)[B + \frac{\lambda}{T_\varepsilon {l_0}^2}]\Delta l \tag{2.6}$$

As per definition for $T_\varepsilon$ , $\Delta\phi/2\pi$ represents the number of fringes, $N$, that will be produced due to the change in length, $\Delta l$ , and it is expressed as:

$$N = \frac{\Delta\phi}{2\pi} = [\frac{B}{\lambda} + \frac{1}{T_\varepsilon {l_0}^2}]\Delta l = \alpha\Delta l \tag{2.7}$$

Where $\alpha = [\frac{B}{\lambda} + \frac{1}{T_\varepsilon {l_0}^2}]$

Equation (2.7) provides the fundamental relationship between deformation and the number of fringes resulting from it. Since this relationship is linear, it is possible to develop a calibration constant relating the number of fringes to deformations.

## 2.2 Crack Tip Opening Displacement Sensor

Sensitivity of the fiber optic sensor described in the preceding section is directly proportional to the gauge length ,$l_o$, of the Hi-Bi fiber[11, 13]. Other terms in Equation (2.7), i.e., $\lambda$, and $B$ are constants that depend on the wavelength of laser and optical properties of the fiber.

In comparison with the effect of $\Delta l$, variations in optical properties ($\lambda$ and $B$) do not influence the number of fringes, $N$, in a significant manner. Since $\Delta l = \varepsilon l_o$, for a number of optical fibers subjected to the same level of strain intensity, longer gauge lengths ($l_o$) produce larger deformations.

According to Equation (2.7), this will in turn increases the number of fringes, and therefore the resolving power of the sensor for the given strain level. Displacements associated with microcracking in concrete are in the order of few micrometers.

As shown in Figure 2.2(a), cracking is a localized phenomenon, and deformations associated with microccracking in concrete specimens occur over a very short length of the optical fiber (few millimeters). Therefore, the Hi-Bi optical fiber, as described above does not provide sufficient resolution for measurement of crack tip opening displacements.

However, it is possible to produce a very sensitive CTOD transducer by increasing the gauge length of the optical fiber through the specific coil arrangement

shown in Figure 2.2(b). In this configuration, the optical fiber coil is embedded in concrete on the plane perpendicular to the direction of crack opening displacements at the notch tip. The gauge length, $l_o$ , is chosen by the circular bend diameter, and the number of loops in the coil. If $n$ represents the number of loops in the coil, and $r$ is the diameter of the circular bend then $l_o = n(2\pi r)$ .

Sensitivity of the transducer can be most efficiently increased by increasing the number of loops in the coil. This arrangement does not produce a bulky transducer, since optical fibers are extremely thin (typically 200 micron in diameter).

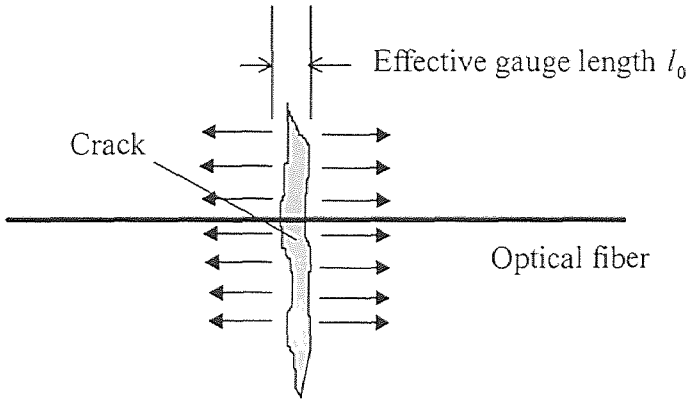


(a) Straight optical fiber geometry.

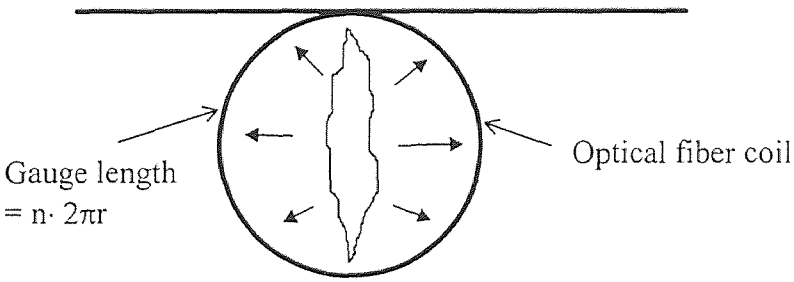


(b) Optical fiber sensor coil.

**Figure 2.2** Geometric relationship between a crack and an embedded optical fiber.

# CHAPTER 3

# EXPERIMENTAL PROCEDURE

## 3.1 Experimental Investigation

The experimental program was designed for evaluation of the fiber optic CTOD transducer. Experiments involved testing standard three-point-bend center-edge-notched concrete beams. Typical beam dimensions and the geometry of embedded optical fiber with respect to the notch tip are given in Figure 3.1.

Determination of the number of loops, $n$, in the fiber optic coil was based on experiments with three different sensors, each with a different $n$. A calibration procedure was developed in order to determine the calibration constant relating the number of fringes corresponding to a unit displacement.

## 3.2 Specimen Preparation

Specimens were made with the mix proportions of : 1.0:1.1:0.35:0.1(cement:sand:coarse aggregate:water:silica fume by weight). Type III cement meeting ASTM SPEC C-150 was used to get high early strength. The sand conforming with ASTM C33 was used.

The F.M(Fineness Modulus) was 2.79 and absorption was measured at 0.5%. Coarse aggregate having F.M 6.43 was utilized. A superplasticizer at 2.2 liter per 220 lb. of (cement + silica fume)was added at the end of mixing to obtain workability. Specimen dimension was 3x3x20 inch. Specimen were cast in plexiglas molds.

After casting, the specimens were cured in the fog room(100% relative humidity) for two weeks. All specimens were air dried for couple of days before testing. Also some

cylinders were cast in order to obtain the compressive strength($f'_c$) and the modulus of elasticity(E) of the concrete.

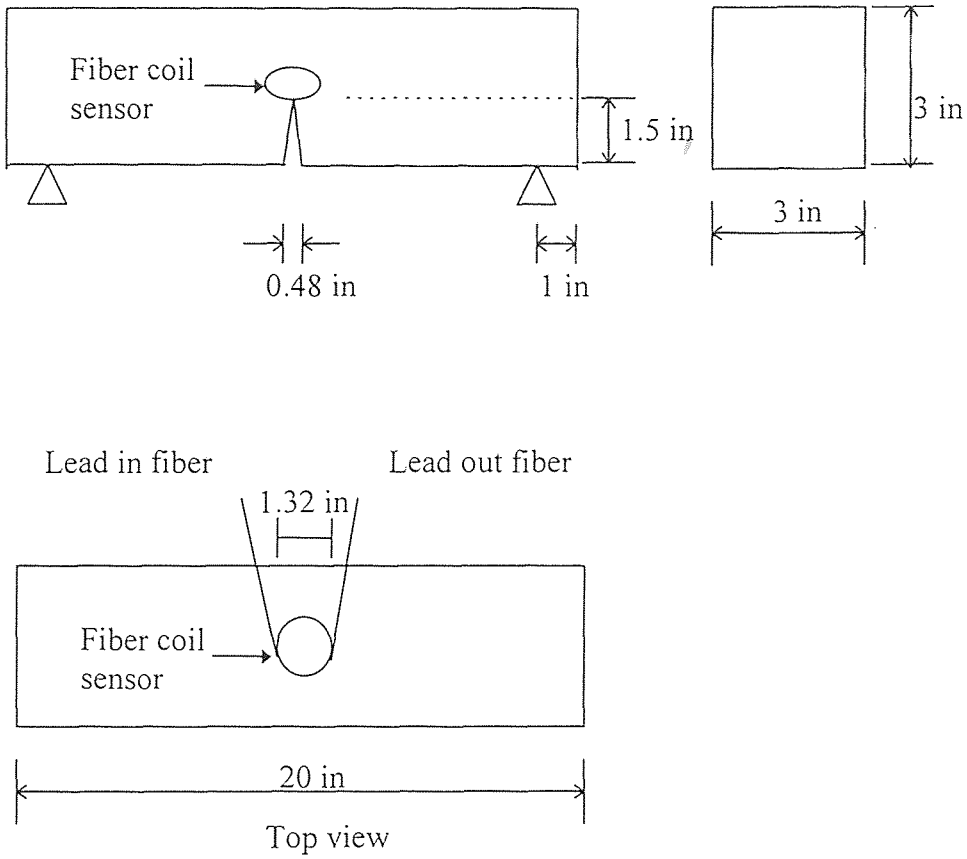


**Figure 3.1** Typical beam dimensions and location of the embedded optical fiber in concrete.

### 3.3 Calibration

Correlation between displacements and the corresponding fringes is accomplished by way of calibration. The calibration constant, $\alpha$, as given in Equation (2.8) can be found from a plot of $N$ versus $\Delta l$. The configuration shown in Figure 3.2 corresponds to the

calibration process, and for simplicity it does not include the laser and polarization optics. Accordingly, the crack tip opening displacements through the thickness of a specimen are simulated by the separation of cylinder halves. Crack opening displacements along the crack profile in concrete are not uniform mainly due to aggregate interlock. Therefore, the calibration similitude presented in this study corresponds to an average CTOD value along the crack profile.

The calibration process involves using portland cement paste for affixing the fiber optics around two cylinder halves of diameter 1.32 in. Polarization optics at the optical input and output will be explained in the following section of this thesis. A motorized micrometer positioner separates the cylinder halves, and an LVDT measures the separation. The cement paste coating employed for affixing the optical fiber to the calibration cylinder prevents slippage and simulates bonding of the fiber in concrete.

A data acquisition board is employed for receiving the optical fringe (Figure 3.3), as well as data transmitted by the LVDT due to the separation of the cylinder halves (Figure 3.4). As shown in Figure 3.5, the calibration constant, $\alpha$, can be obtained by calculating the slope of the line relating the number of fringes to displacements. Data presented in Figure 3.3, 3.4, 3.5 corresponds to the fiber coil with 7 loops ( $n = 7$ ). Figure 3.6, 3.7, 3.8 depict calibration data for the fiber coil with 5 loops ( $n = 5$ ), and another set of experiments were also performed with a fiber coil consisting of only 3 coils(Figure 3.9, 3.10, 3.11). The sensor with n=7 provided sufficient sensitivity. As shown in Figure 3.12, the sensitivity of the sensor(calibration constant) is directly related to the number of loops in the optical fiber coil. The linear correlation depicted in Figure 3.12 provides a useful tool for design of coil sensors.

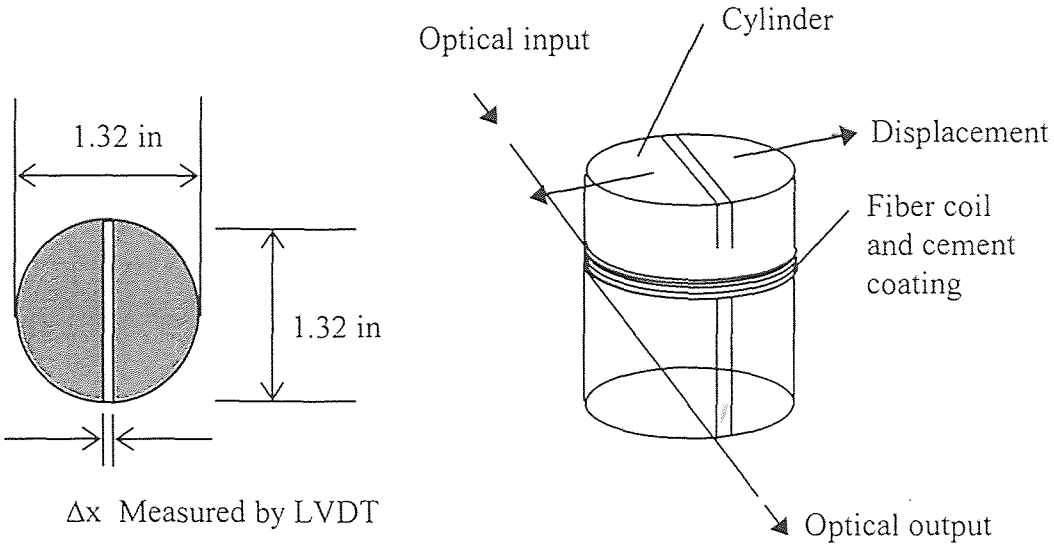


**Figure 3.2** Calibration setup.

### 3.4 Testing Procedure

The experimental setup consisted of optical system, testing machine, and data acquisition. The optical system consisted of a 633 nano-meter laser source, two quarter-wave plates, two plane-polarizers, two fiber adapters for connecting the polarization maintaining fiber to the quarter-wave plates, a photo detector, and the signal amplifier.

The polarized beam from the polarizer was changed into circularly polarized light through the quarter-wave plate. The polarization maintaining fiber was connected to the quarter-wave plate via the fiber connector. Hi-Bi optical fibers were used. The output signal passed through the second quarter-wave plate and analyzer. The optical signal emerging from the optical system propagated into the photo detector. The optical signal was converted into electrical signal at the photo detector. And then this signal was amplified at the amplifier.

Three point bend tests were performed in a closed loop testing system under constant COD rate in order for the crack to grow in a controlled manner. Das-1600 interface board was used for data acquisition. Figure 3.13 represent testing setup. Data included the fiber optic signal, the COD from the LVDT, and load signal from test control system. Data was saved in the computer for data analysis. He-Ne laser was turned on at least one hour prior to the experiment for the laser to reach its stabilized power level.

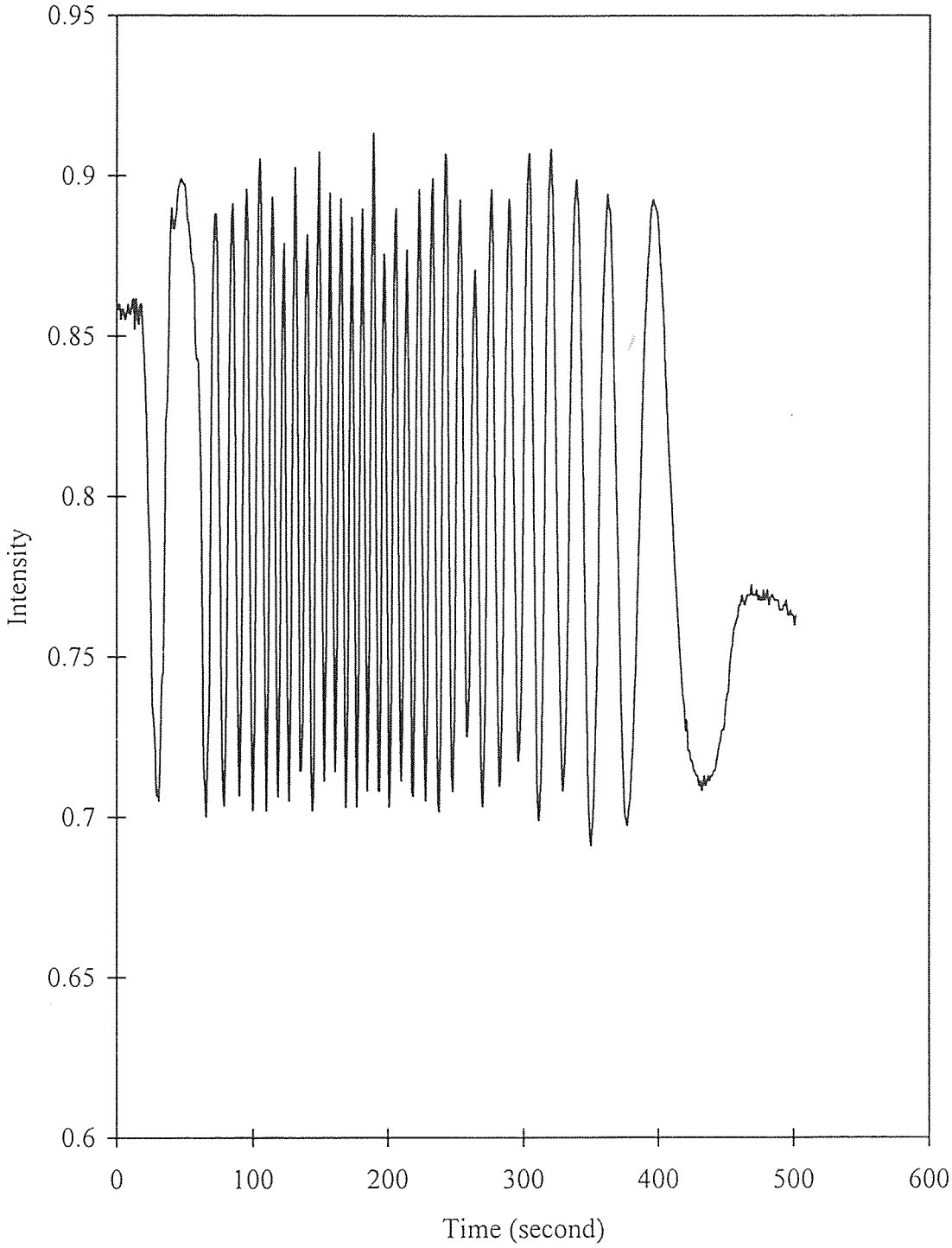


**Figure 3.3** Output of fiber optic coil sensor for n=7.

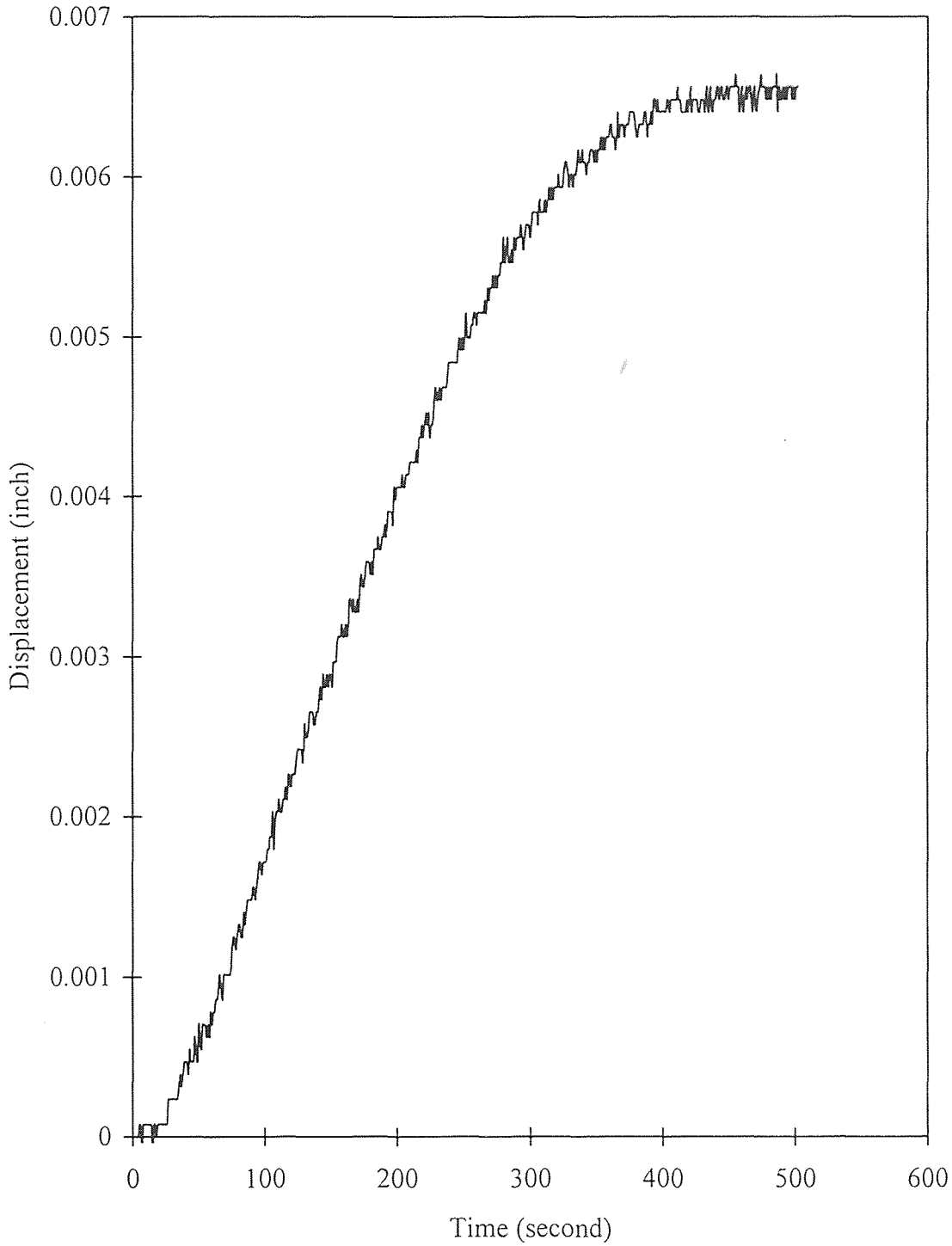


**Figure 3.4** Output of LVDT for n=7.

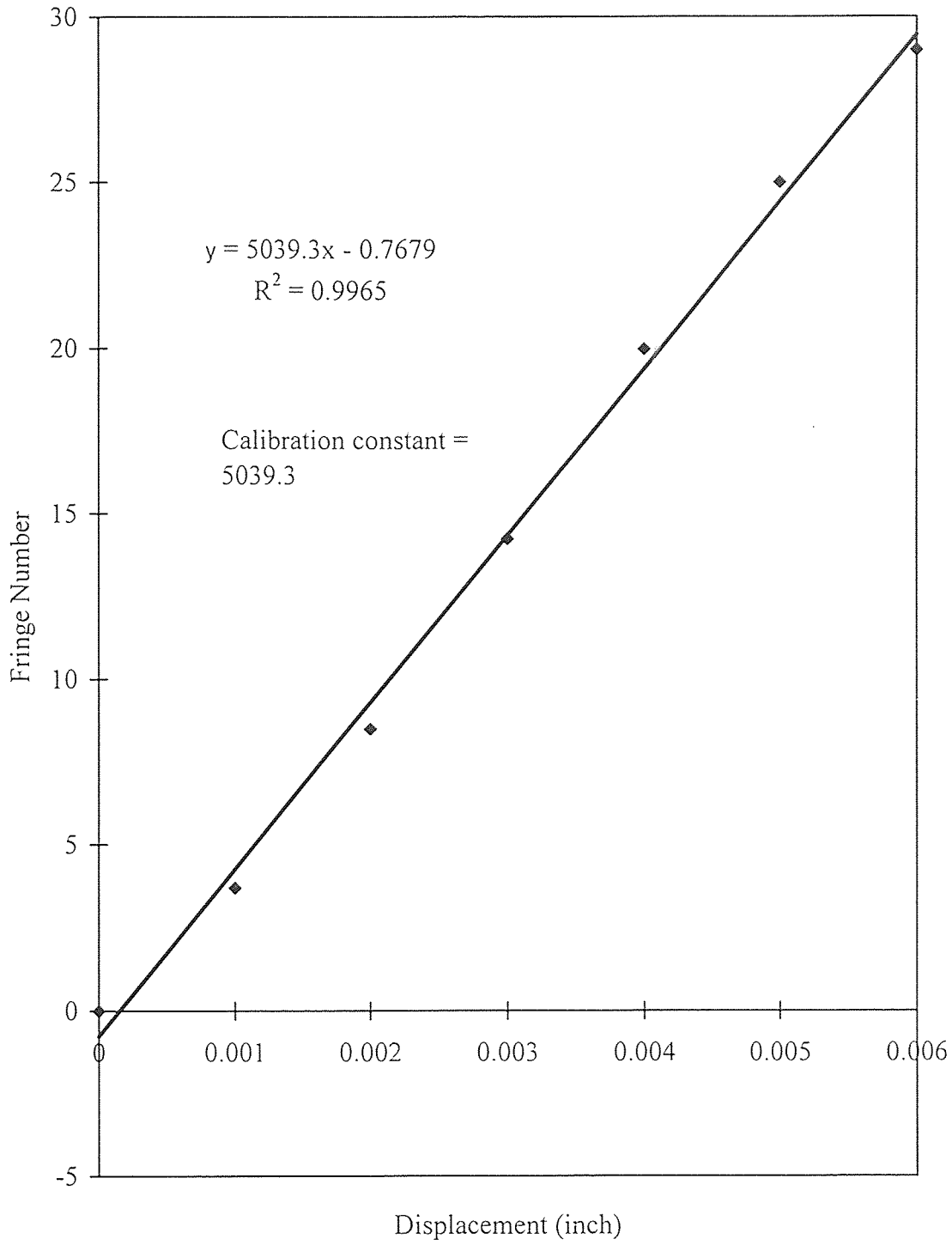


**Figure 3.5** Displacement vs. fringe number for n=7.

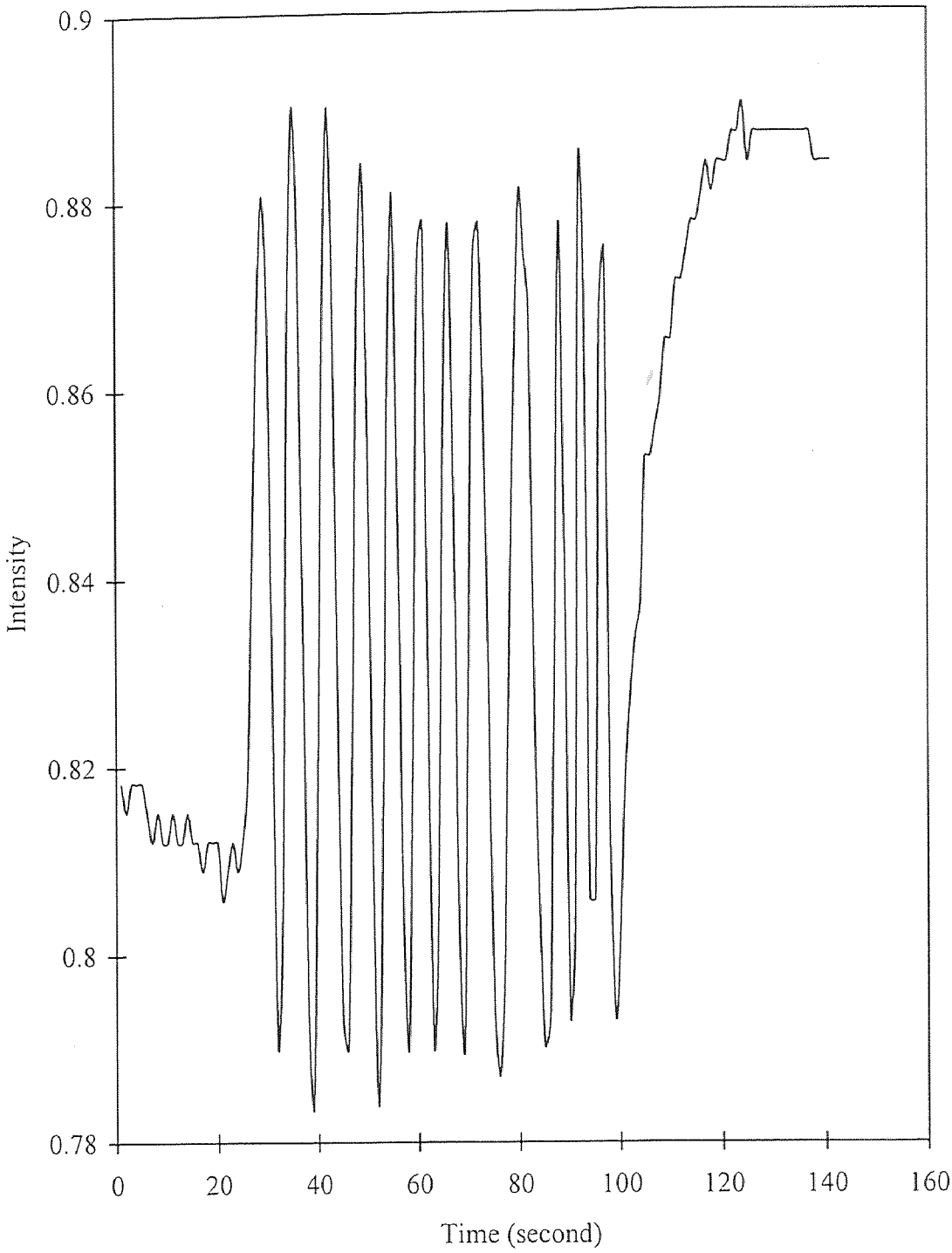


**Figure 3.6** Output of fiber optic coil sensor for n=5.

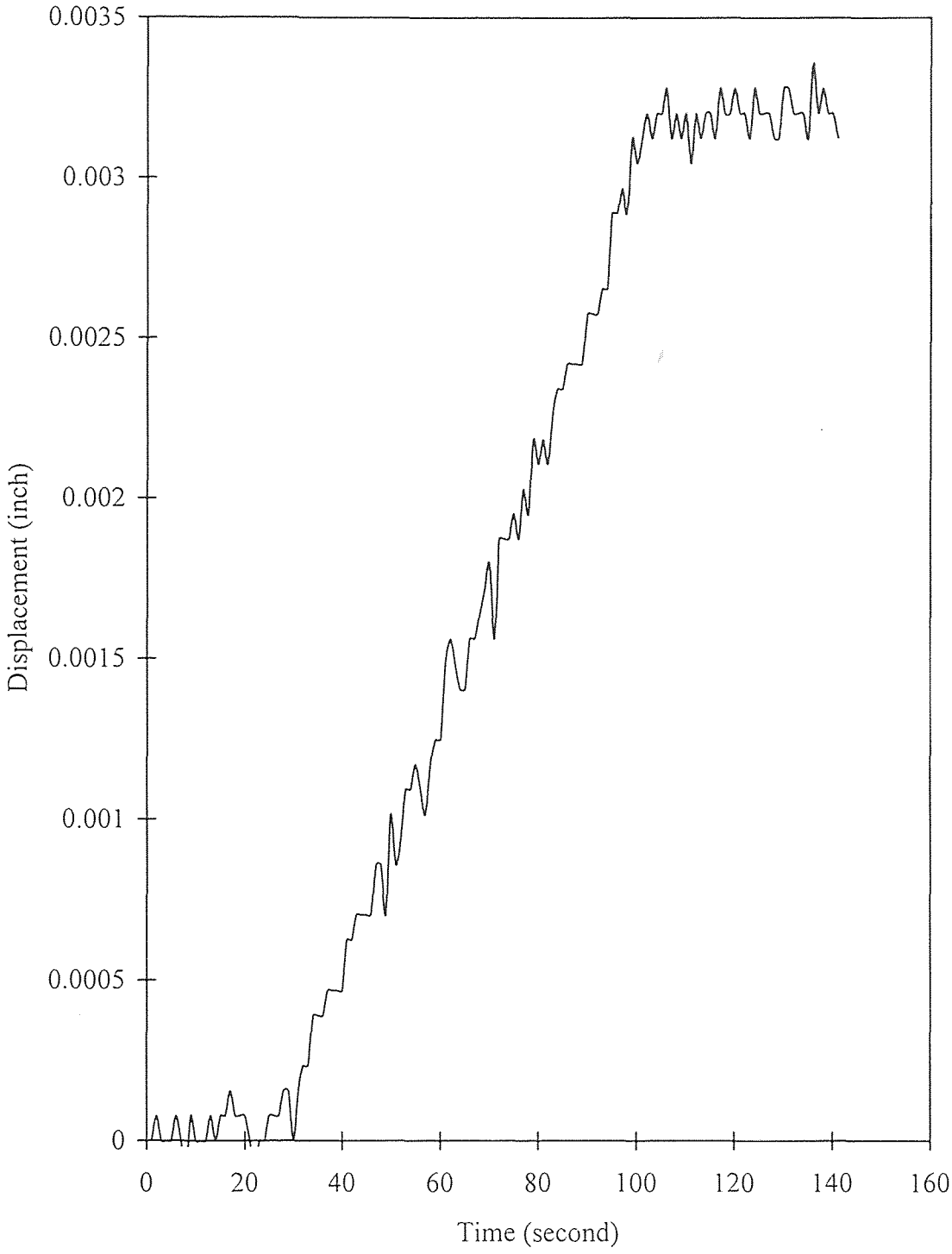


**Figure 3.7** Output of LVDT for n=5.

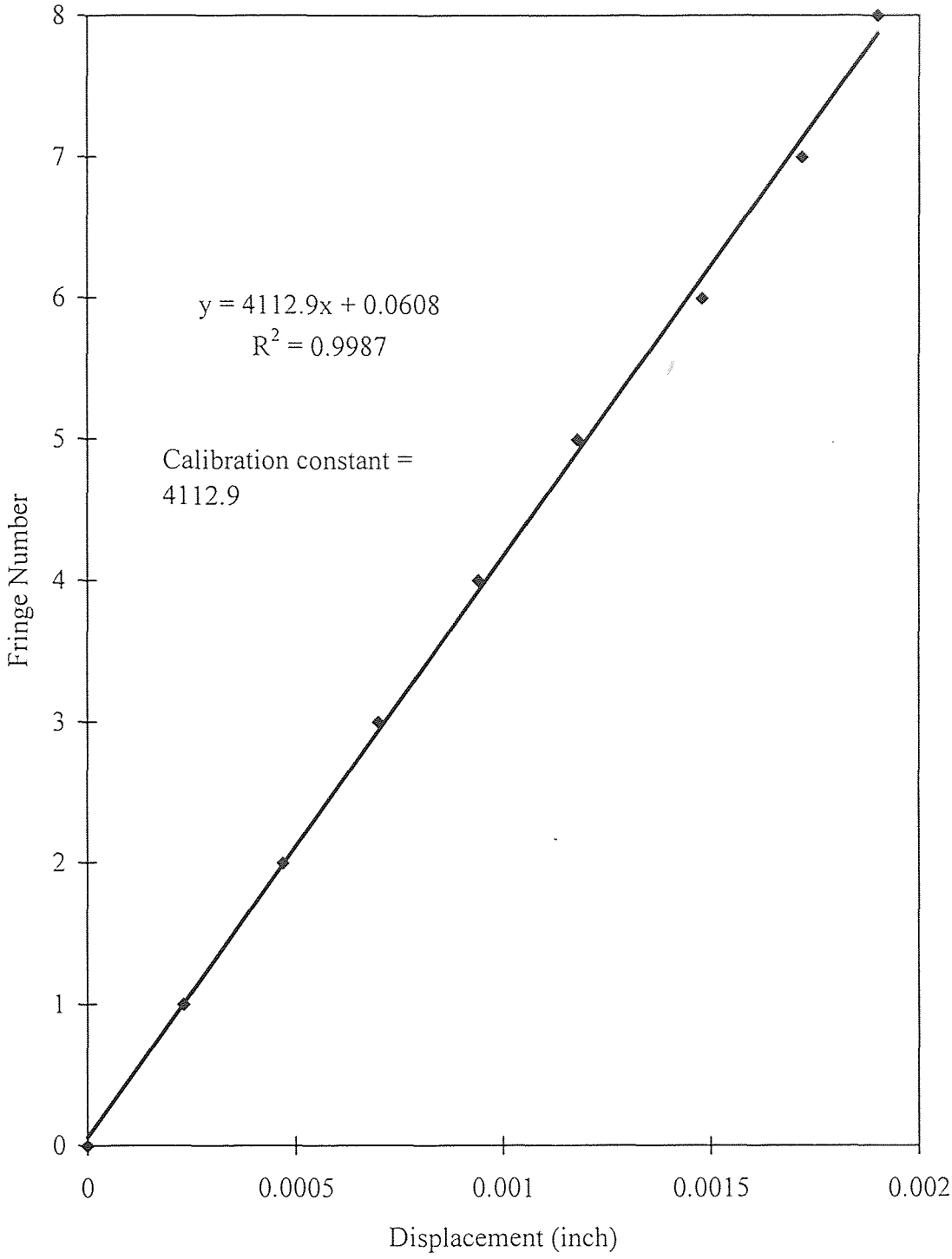


**Figure 3.8** Displacement vs. fringe number for n=5.

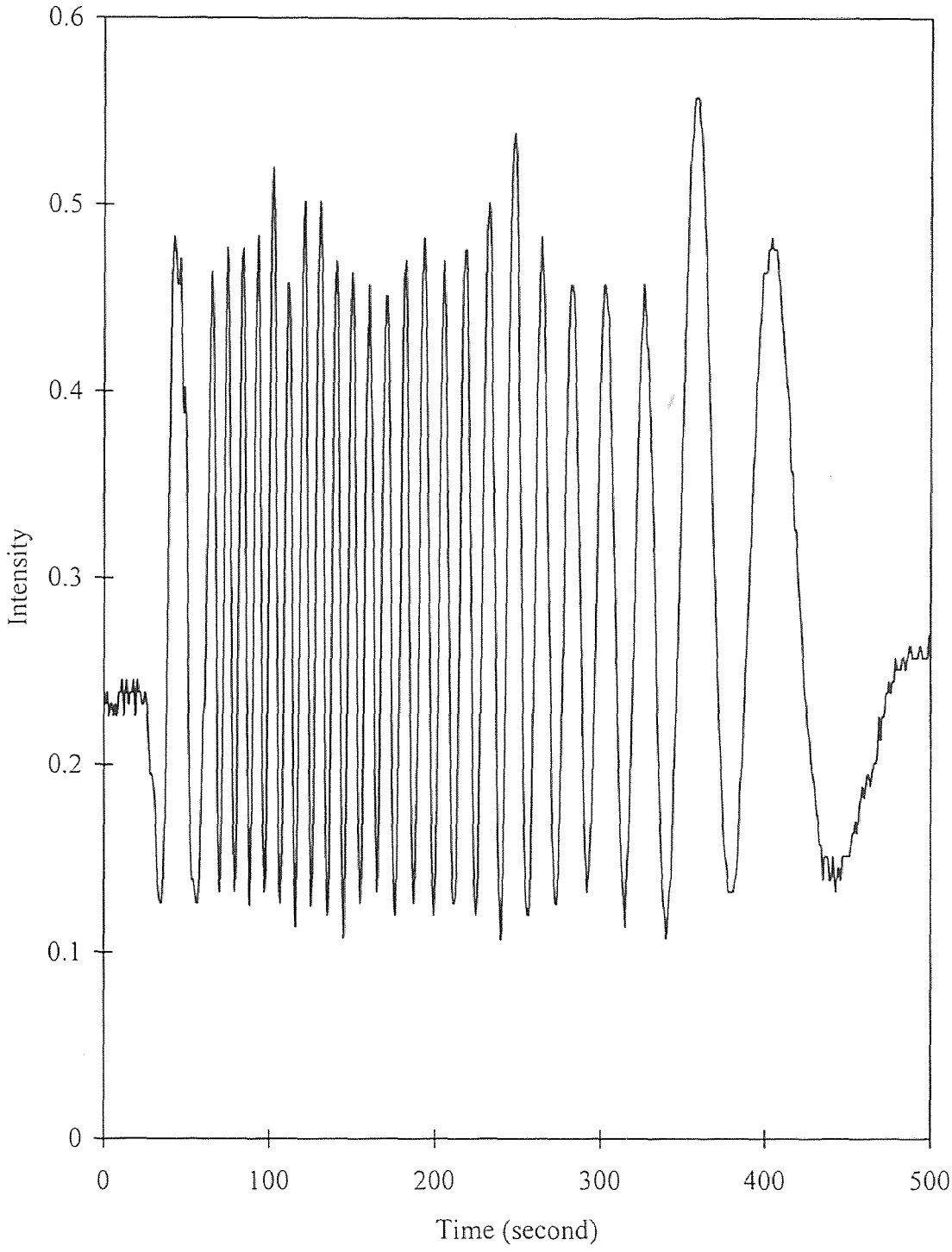


**Figure 3.9** Output of fiber optic coil sensor for n=3.

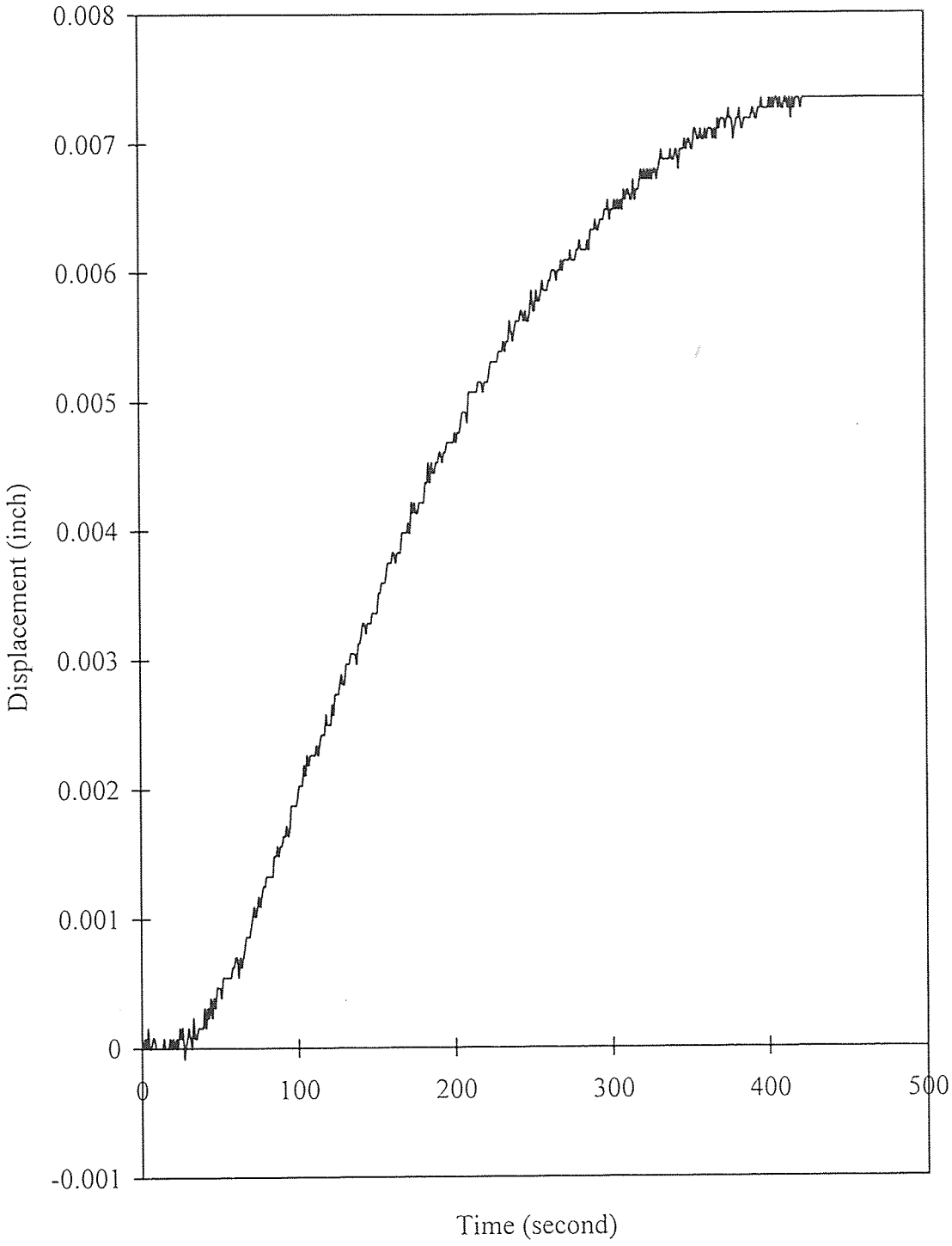


**Figure 3.10** Output of LVDT for n=3.

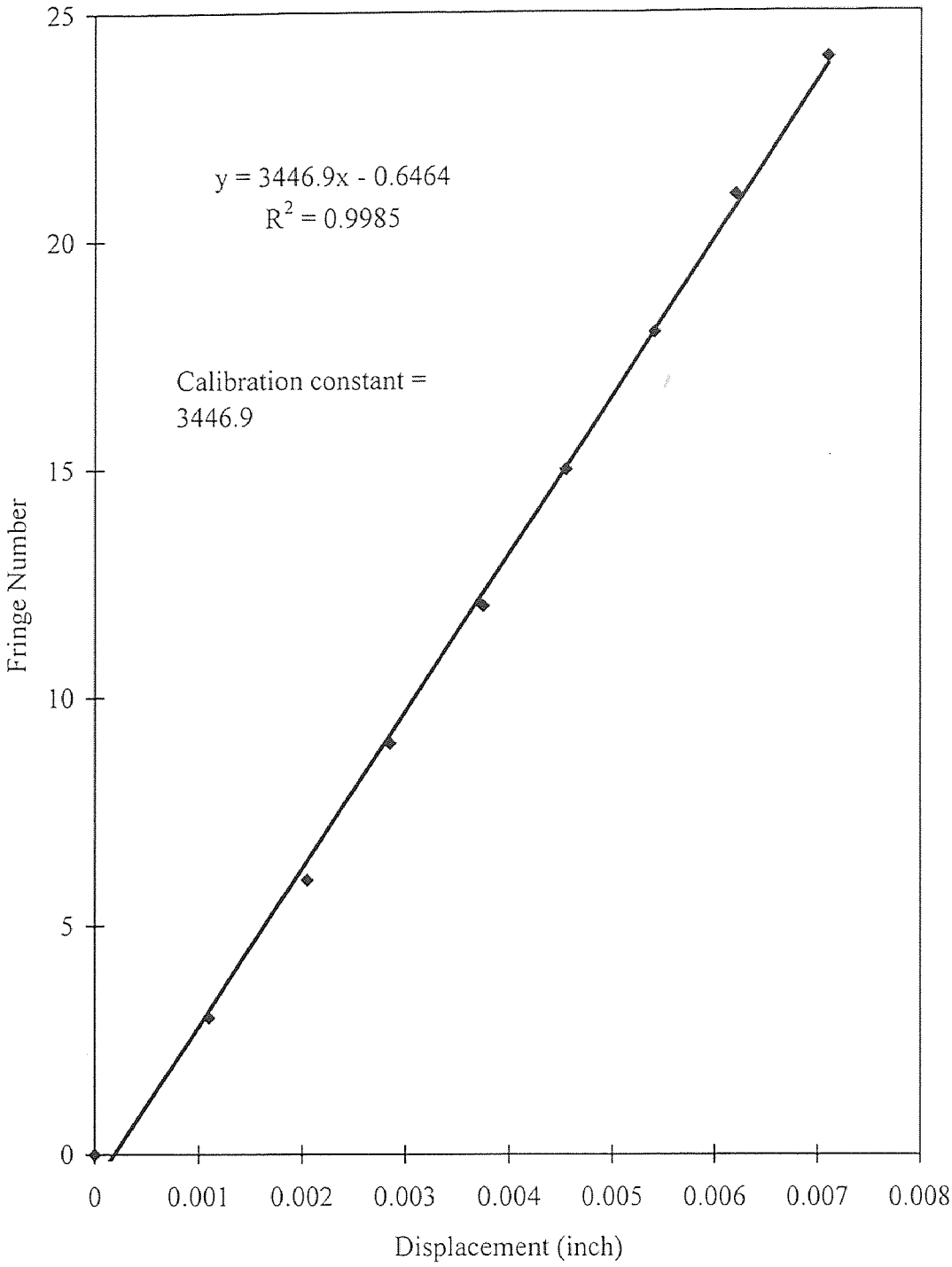


**Figure 3.11** Displacement vs. fringe number for n=3.

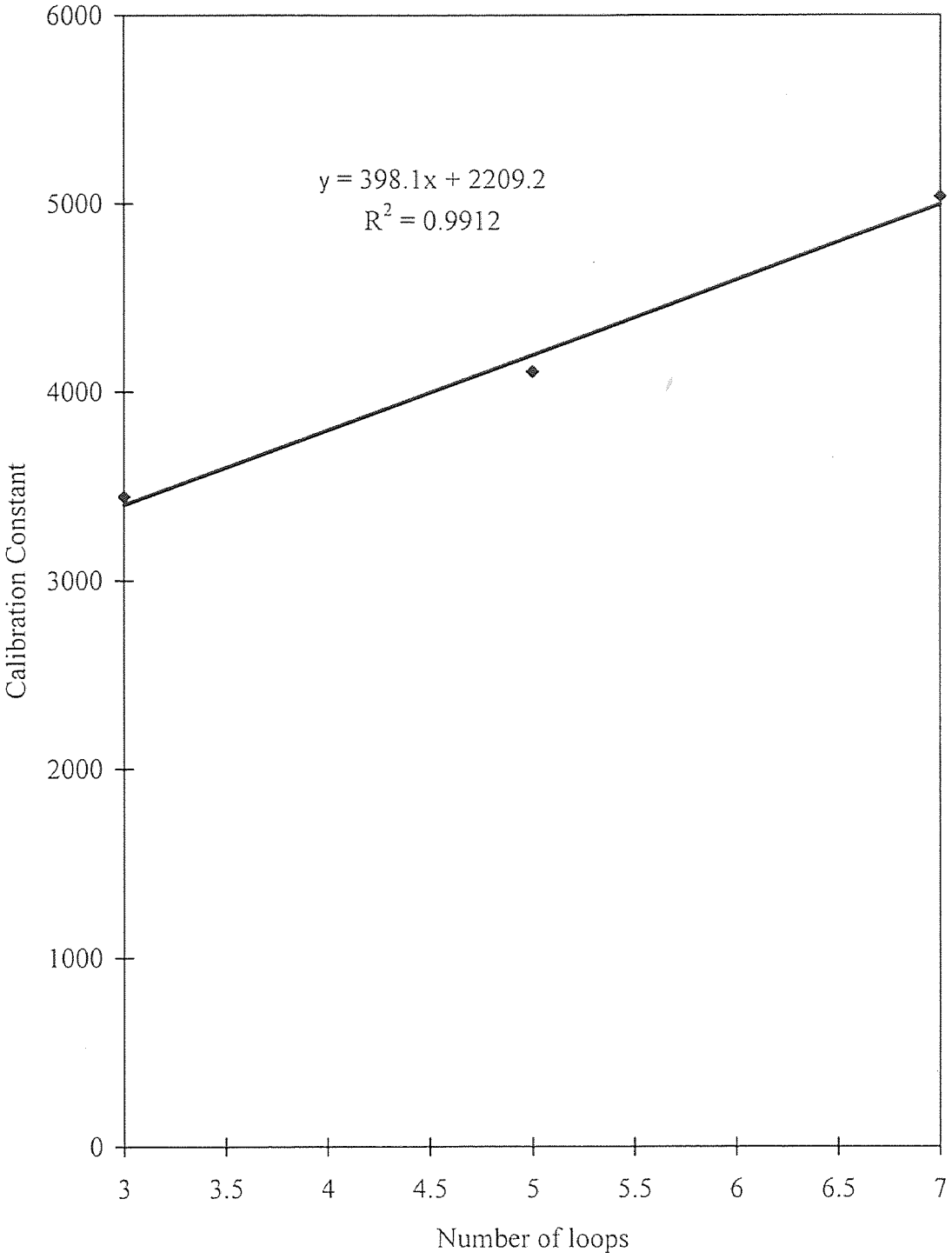


**Figure 3.12** Calibration constant vs. number of loops in the fiber coil.

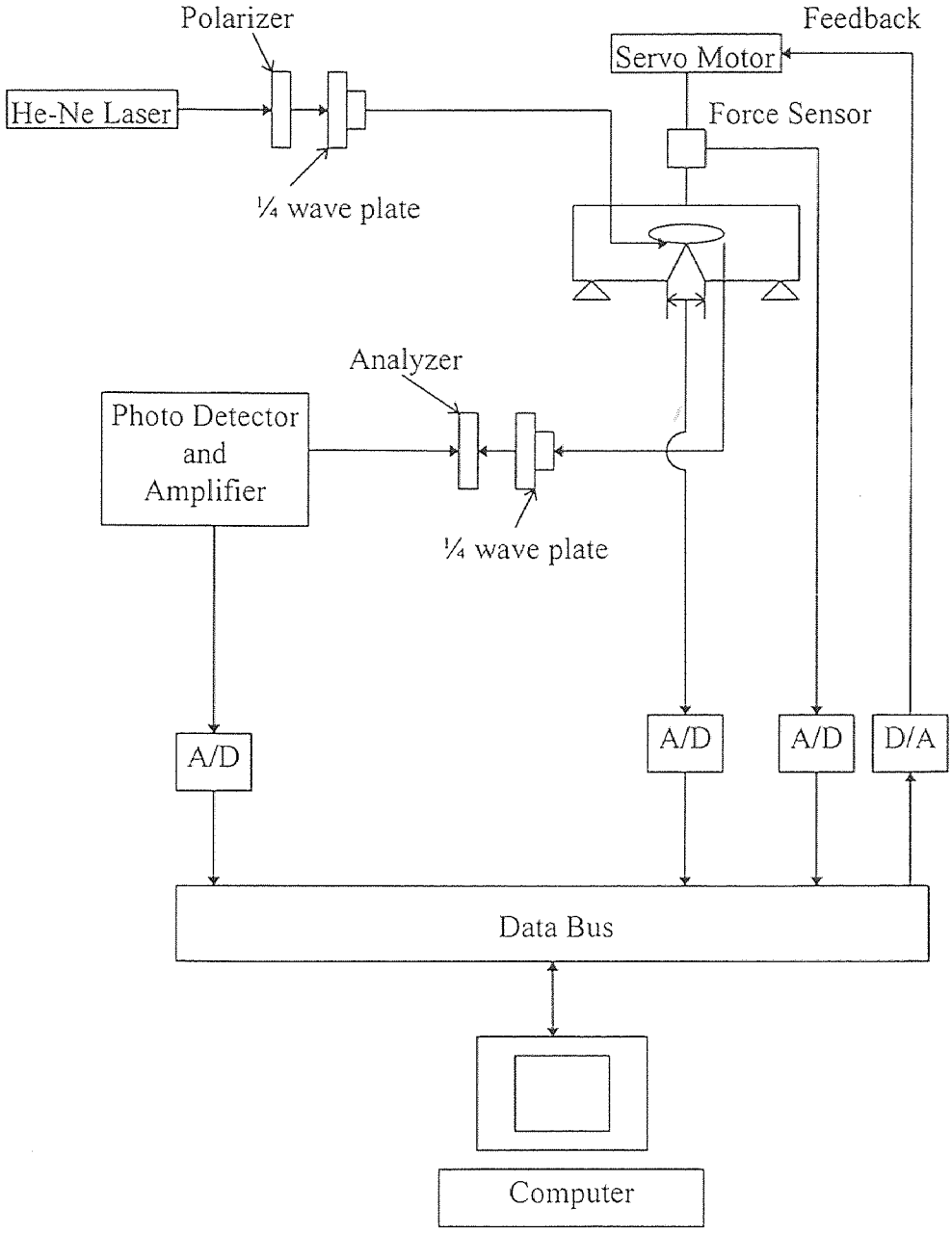


**Figure 3.13** Experimental setup and control system.

# CHAPTER 4

# RESULTS, ANALYSIS AND DISCUSSION

## 4.1 Stress - Strain Curve

A number of concrete cylinders were cast with beams in order to determine the standard 28 days compressive strength of the concrete. The cylinder tests were performed on an MTS 815 closed-loop servo-controlled testing machine with a capacity of 1 million lbf. This machine can test cylinders by using circumferential strain feedback control to get full stress-strain curve. Constant rate of strain was used in the present study experiments, due to the fact that our testing machine is very stiff and capable of controlling the tests under axial control for high strength concrete. The closed-loop system was controlled by personal computer. Data also was acquired by this computer[10]. A feedback signal representing some experimental condition was generated by a transducer and compared with the program signal which represented the desired condition. The difference between these two signal was then used to regulate the servo-valve, which moved the actuator piston to a position minimizing the error signal.

Three 4in x 6in cylinders were tested. The specimens were cast in plastic molds and rodded in three separate layers. The molds were stripped after 24 hr, and then placed in fog room for 2 weeks. Cylinders were capped with sulfur capping compound 1 day before testing. Compressive strength was 7000psi. Figure 4.1 represent the typical stress-strain curve.

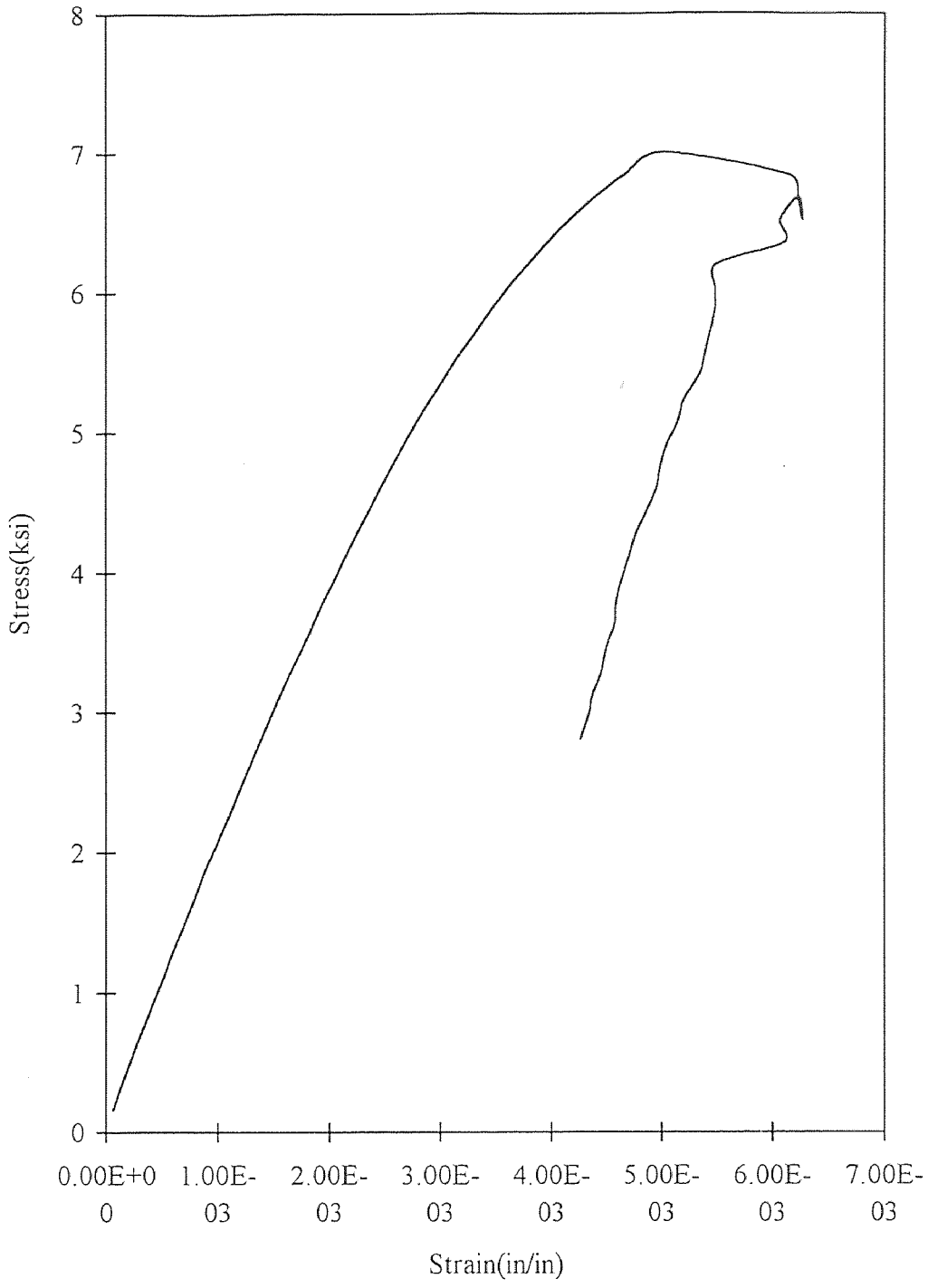


**Figure 4.1** Stress-strain curve.

## 4.2 Results and Discussion

A total of 9 beams, 3 beams for each n=3, 5, 7, were tested. Test results are given in Figures 4.2 through 4.16. Figure 4.17 depicts typical results obtained from a beam test. The results in Figure 4.17 consist of the applied load, and the fiber optics (CTOD) data in the form of optical fringe. The increase in fringe frequency in Figure 4.17 is indicative of increase in CTOD rate during the cracking process. This data indicates that the CTOD rate does not increase in a linear manner, even though, the three point bend tests were performed in a closed loop testing system under constant COD rate. The sharp increase in fringe frequency occurs half way down in the descending branch of the load-time diagram. These results also indicate nonlinear behavior of CTOD with time. One explanation for this stems from inadequate stiffness of the testing machine employed with these experiments. It is also perceived that the half way point in the descending branch of the load-time diagram may correspond to the point were the microcracking region at the tip has formed into a macrocrack. If this is the case, then the visibility of the macrocrack which usually occurs at peak is only a surface phenomenon.

Load, COD, and CTOD data are plotted in Figure 4.18. As shown in this figure, the relationship between the crack displacements (COD and CTOD) and time are nonlinear. The plot of CTOD versus COD in Figure 4.19 indicates that the relationship between the two displacements is linear, and it is possible to use this relationship in fracture models. Load versus COD and CTOD data in Figure 4. 20 are plotted on the same graph for comparison. COD values are much larger than CTOD results mainly due to being further away from the neutral axis (by 1.5 inch). Most fracture models have

employed a critical COD value in the modeling. Relationships such as the one given in Figure 4.19 can be employed to examine the validity of such models.

## 4.3 Conclusions

An optical fiber sensor is developed that can be embedded within cementitious composites for the measurement of crack tip opening displacements. A calibration technique was developed for conversion of optical data to the displacements associated with the opening of microcracks. Calibration results indicated that sensitivity of measurements is directly dependent on the number of fiber loops within the sensor coil. By using the present coil geometry, experiments with concrete beams indicated displacement resolving powers as small as 5 microns. Fiber optic data suggest that the crack tip opening displacements are much smaller than the traditionally measured displacements at the crack mouth. The relationship between CTOD and COD was found to be linear. The frequency of optical fringes provided a new tool for measurement of crack growth rate. Fringe frequency data suggest that the steady state crack growth occurs after peak load, and at loads as large as the peak value.

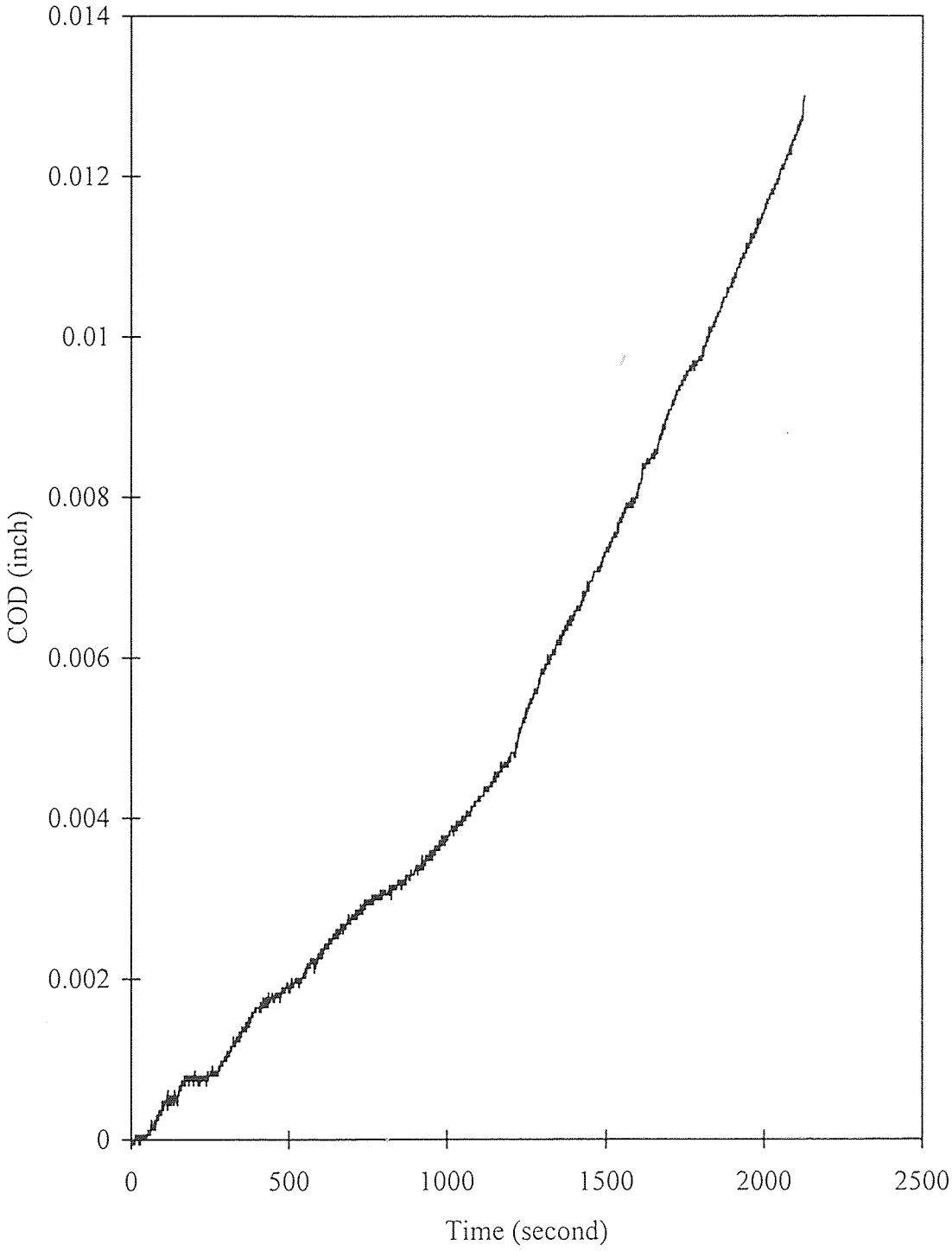


**Figure 4.2** Time vs. COD for n=3.

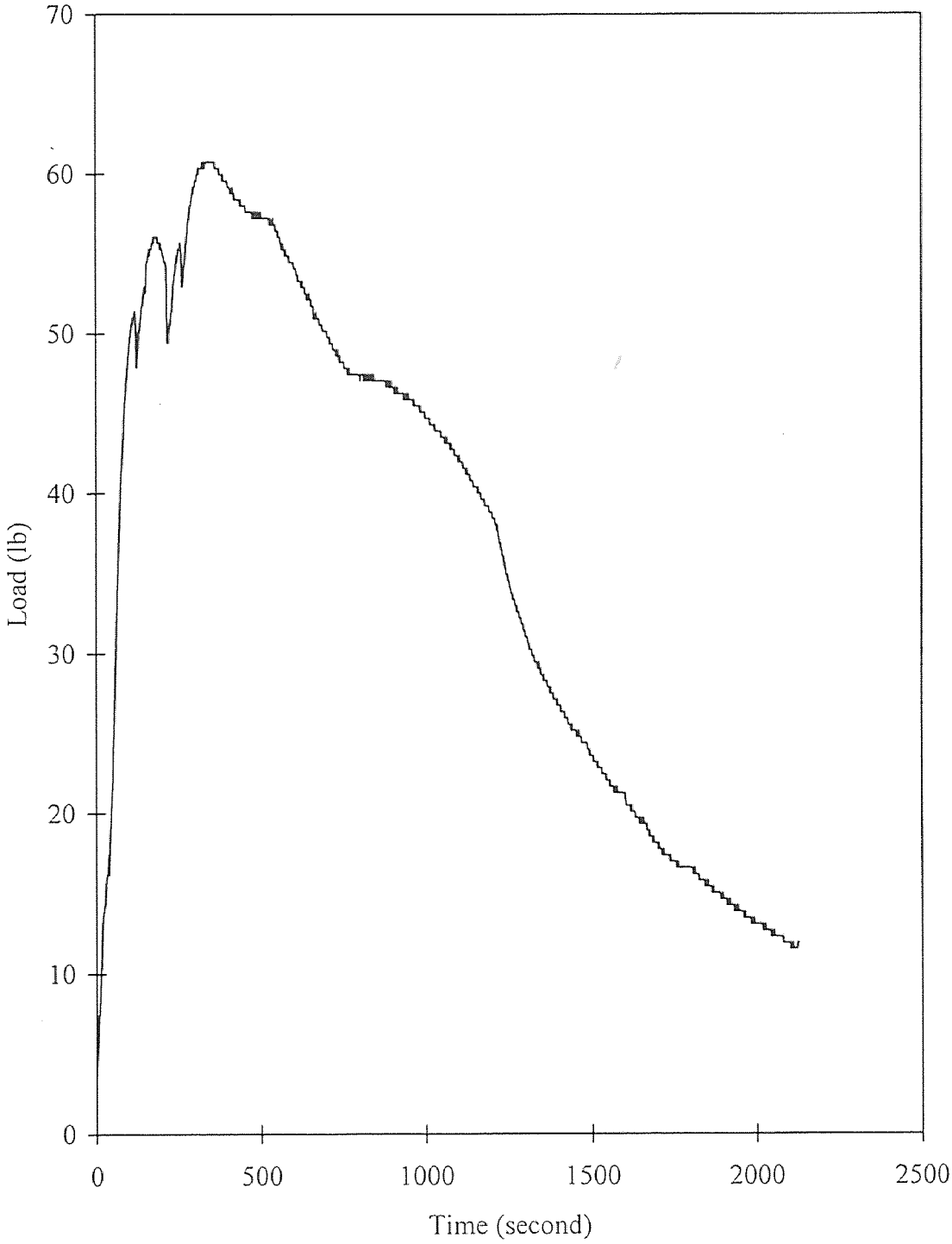


**Figure 4.3** Time vs. load for n=3.

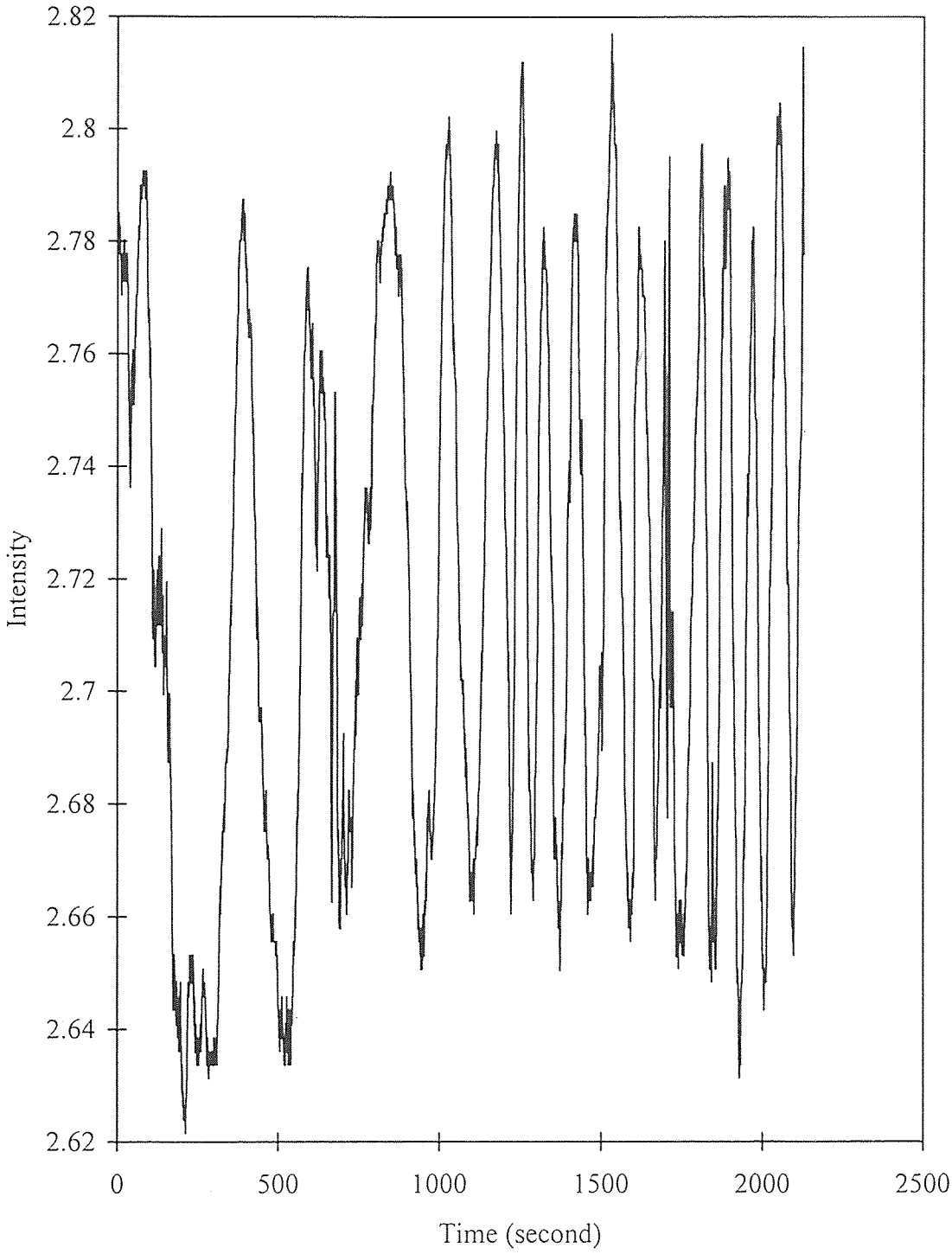


**Figure 4.4** Time vs. intensity for n=3.

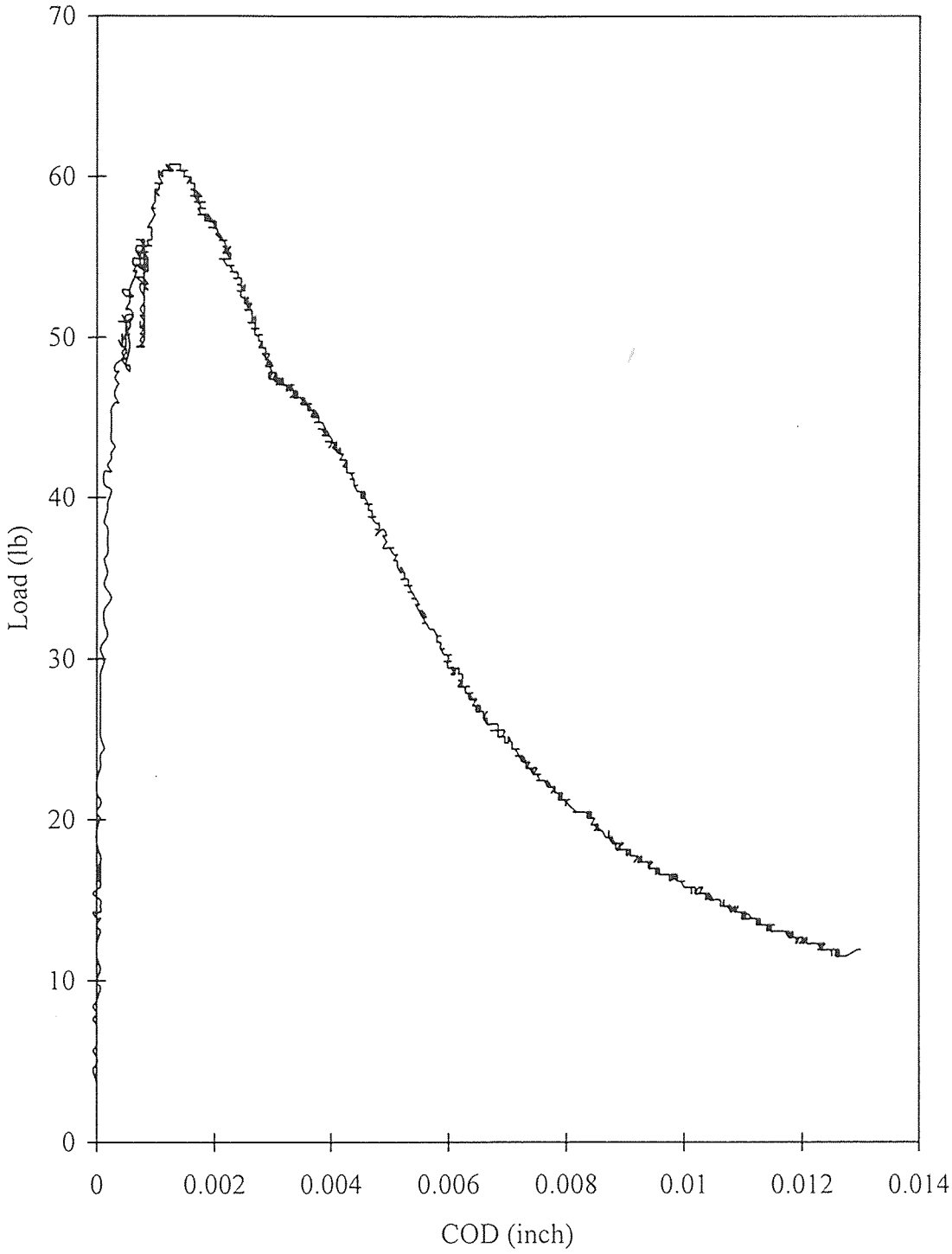


**Figure 4.5** COD vs. load for n=3.

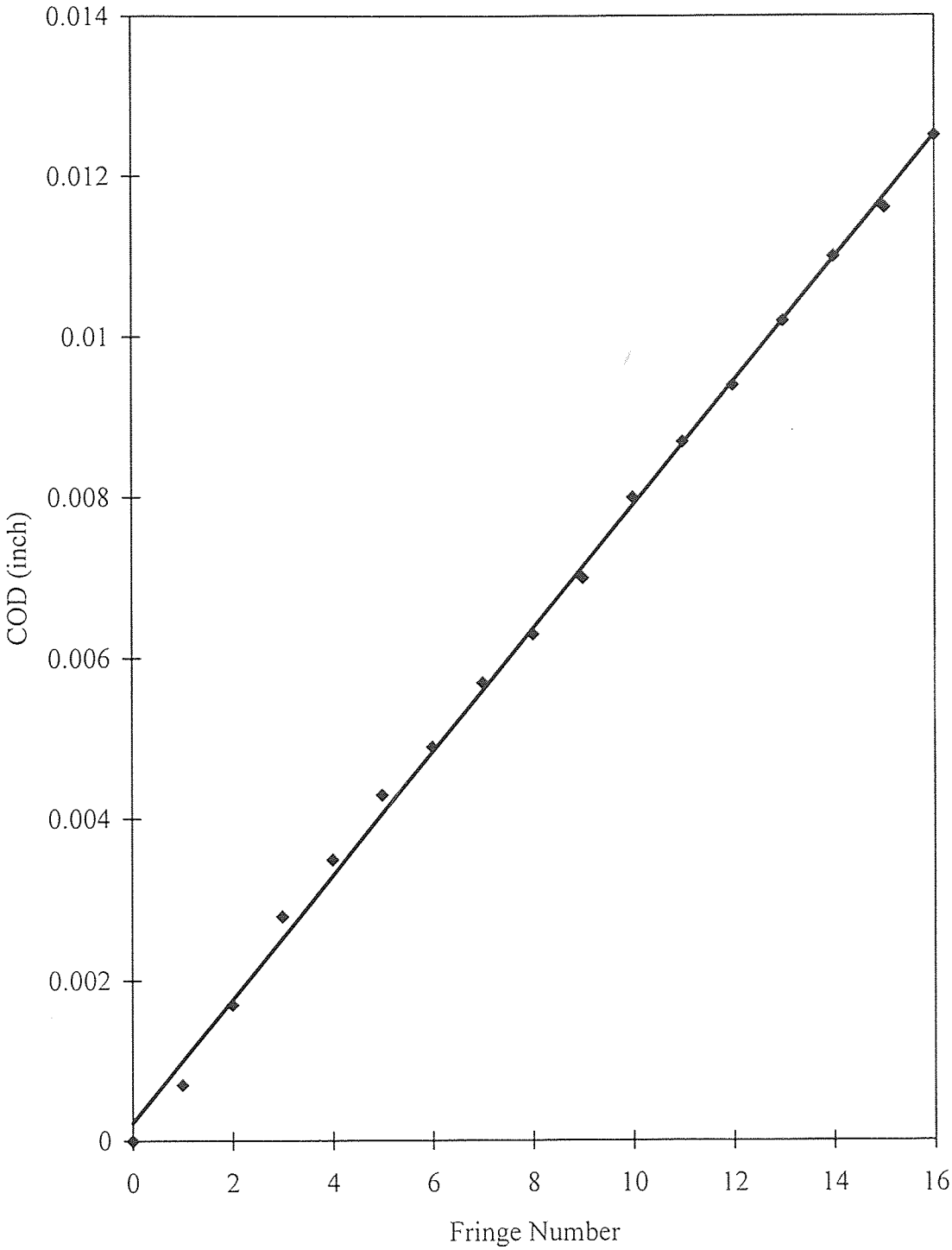


**Figure 4.6** Fringe number vs. COD for n=3.

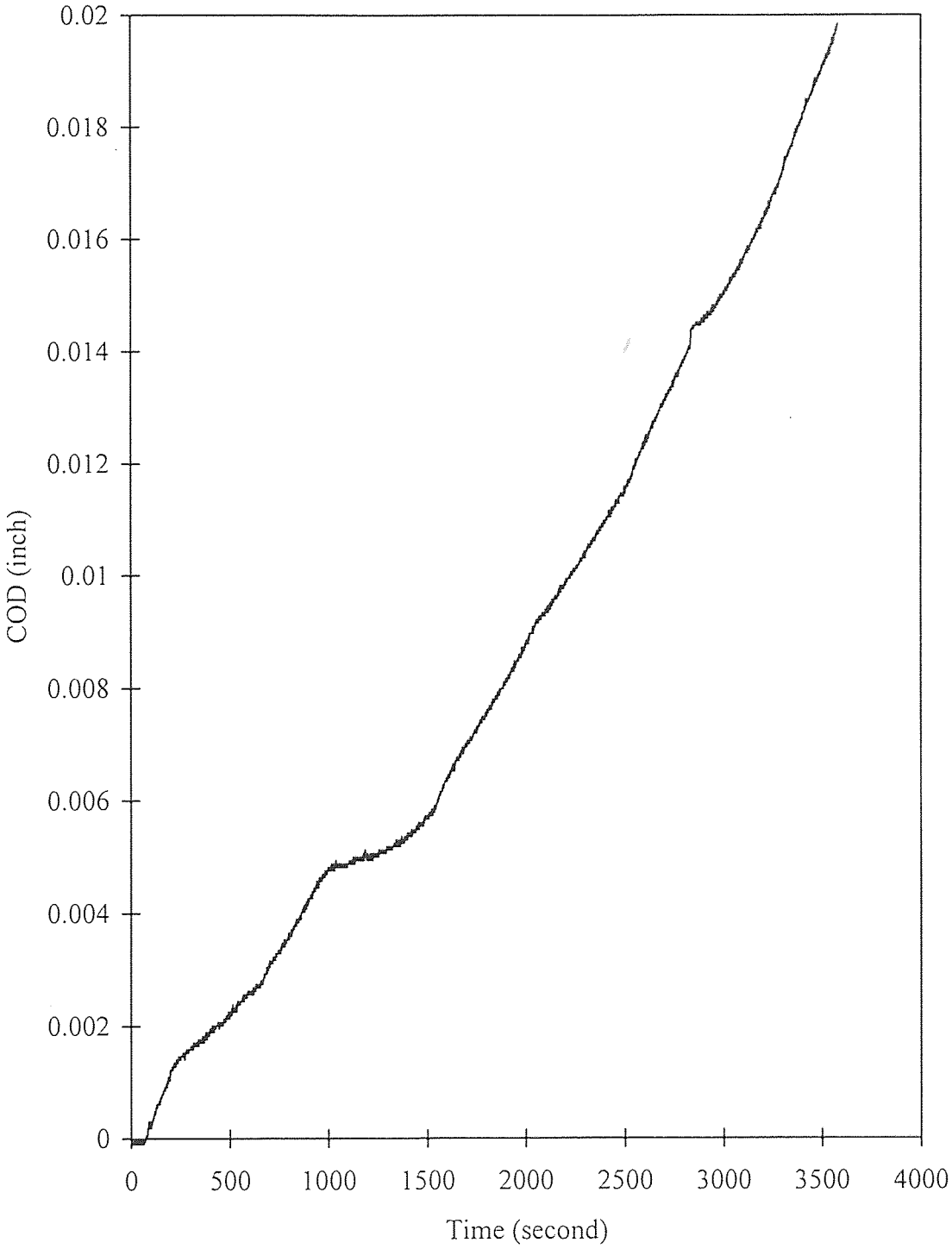


**Figure 4.7** Time vs. COD for n=5.

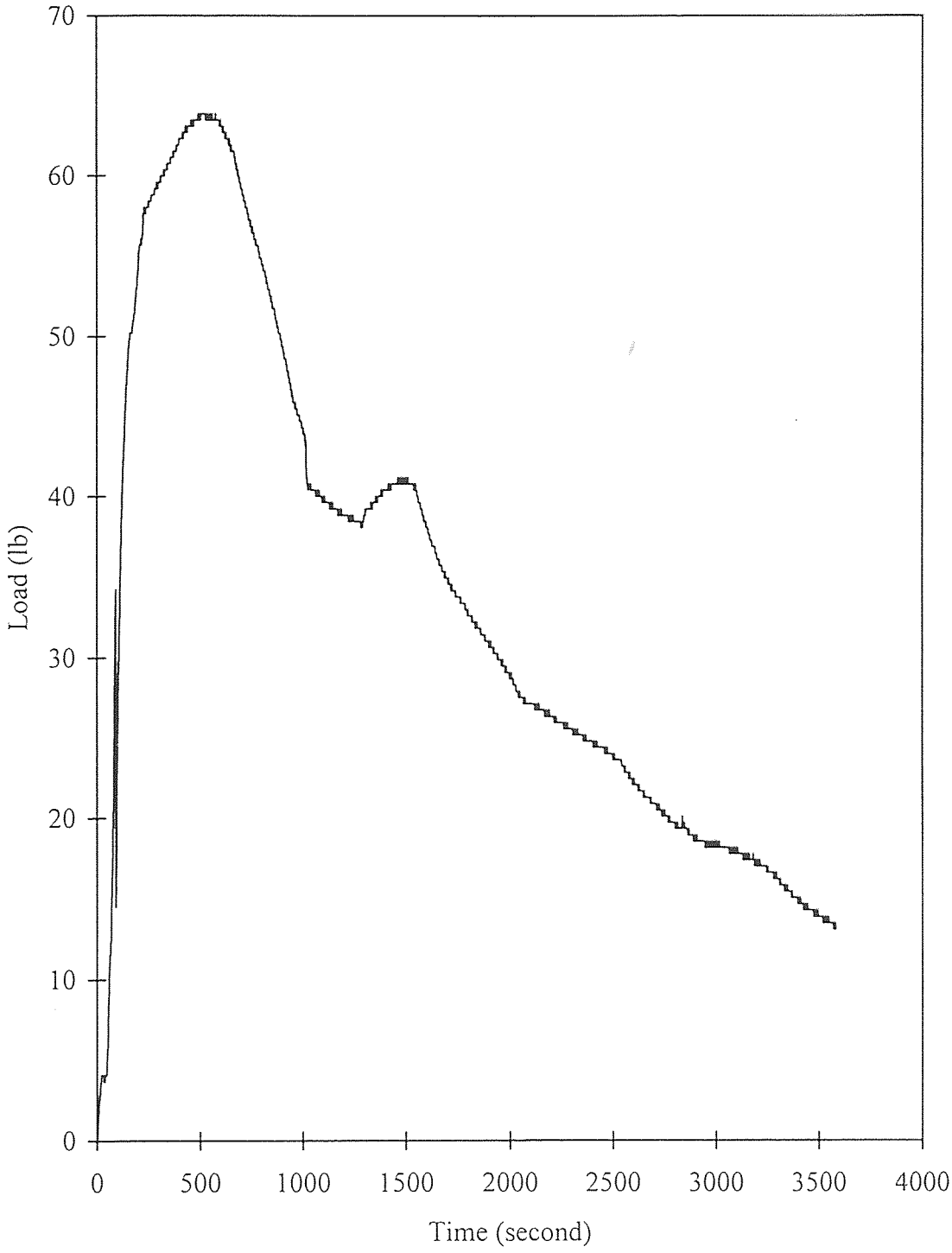


**Figure 4.8** Time vs. load for n=5.

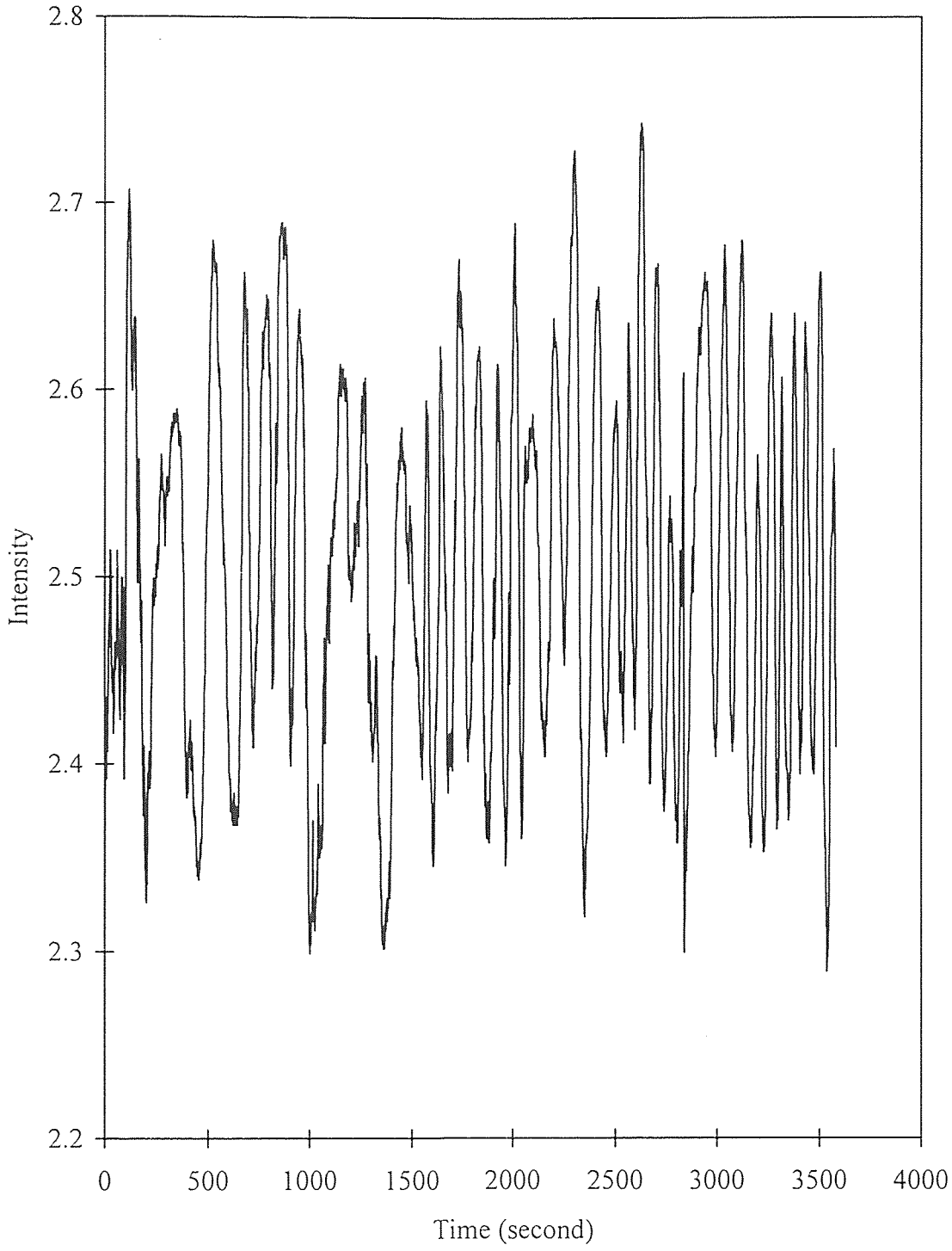


**Figure 4.9** Time vs. intensity for n=5.

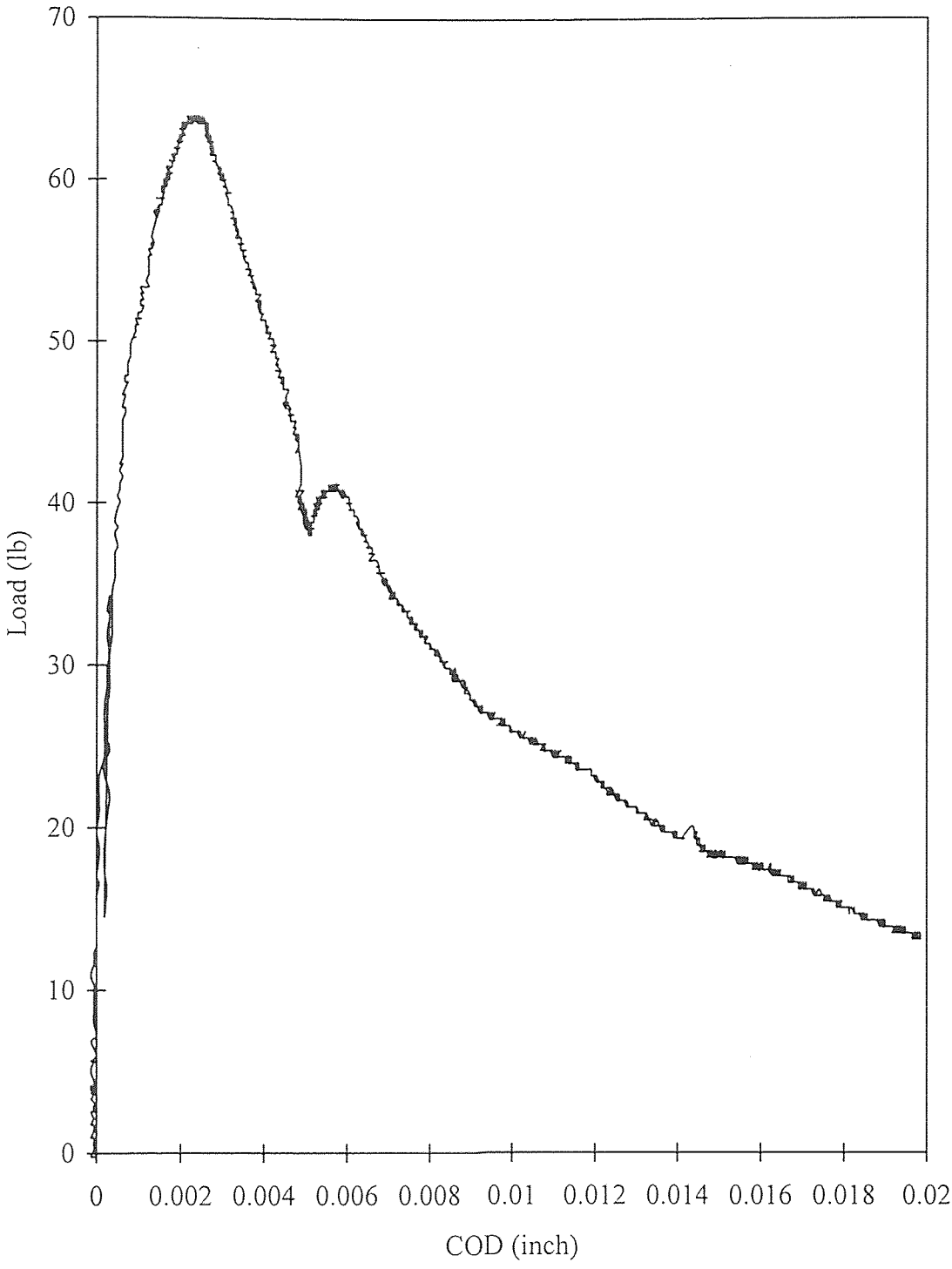


**Figure 4.10** COD vs. load for n=5.

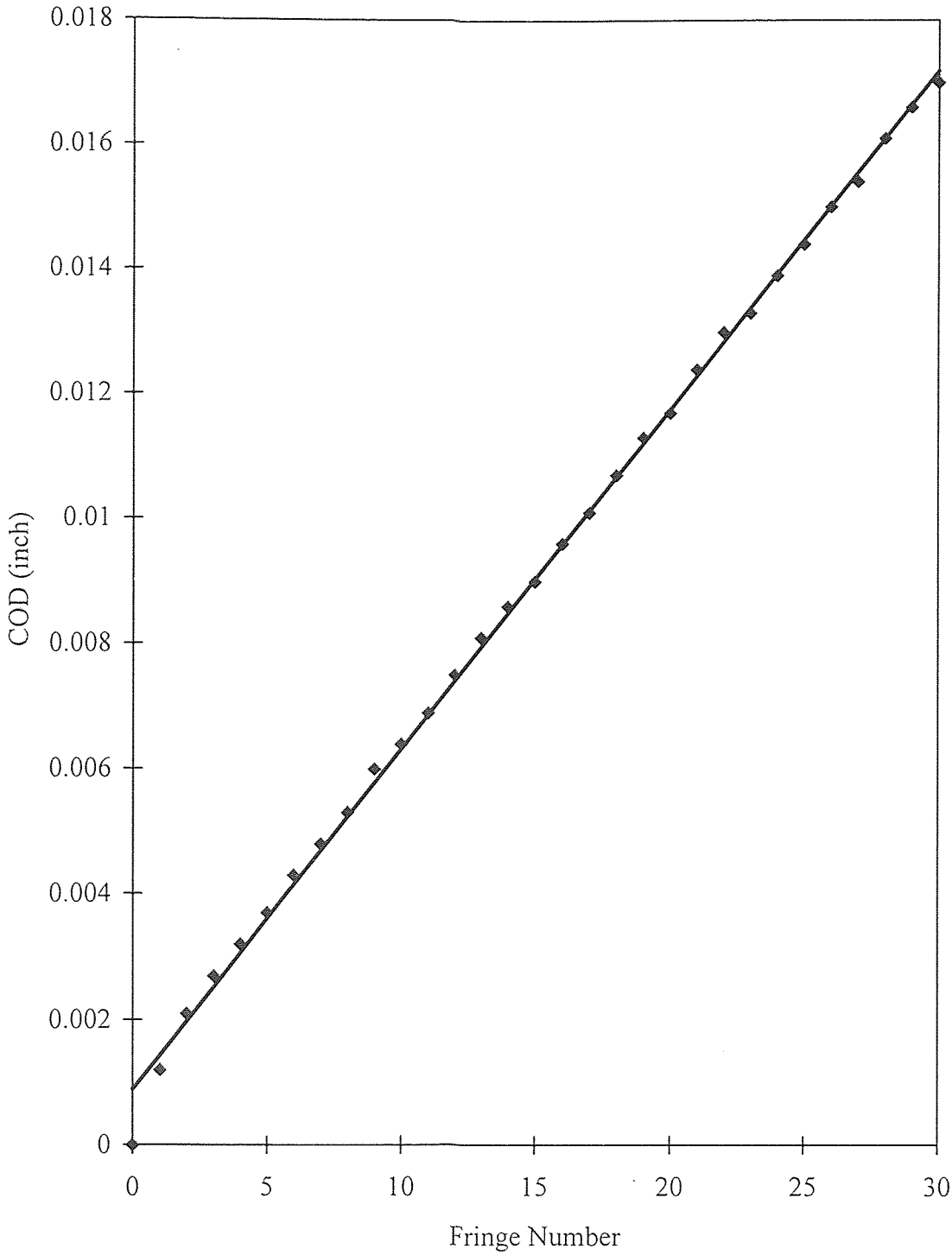


**Figure 4.11** Fringe number vs. COD for n=5.

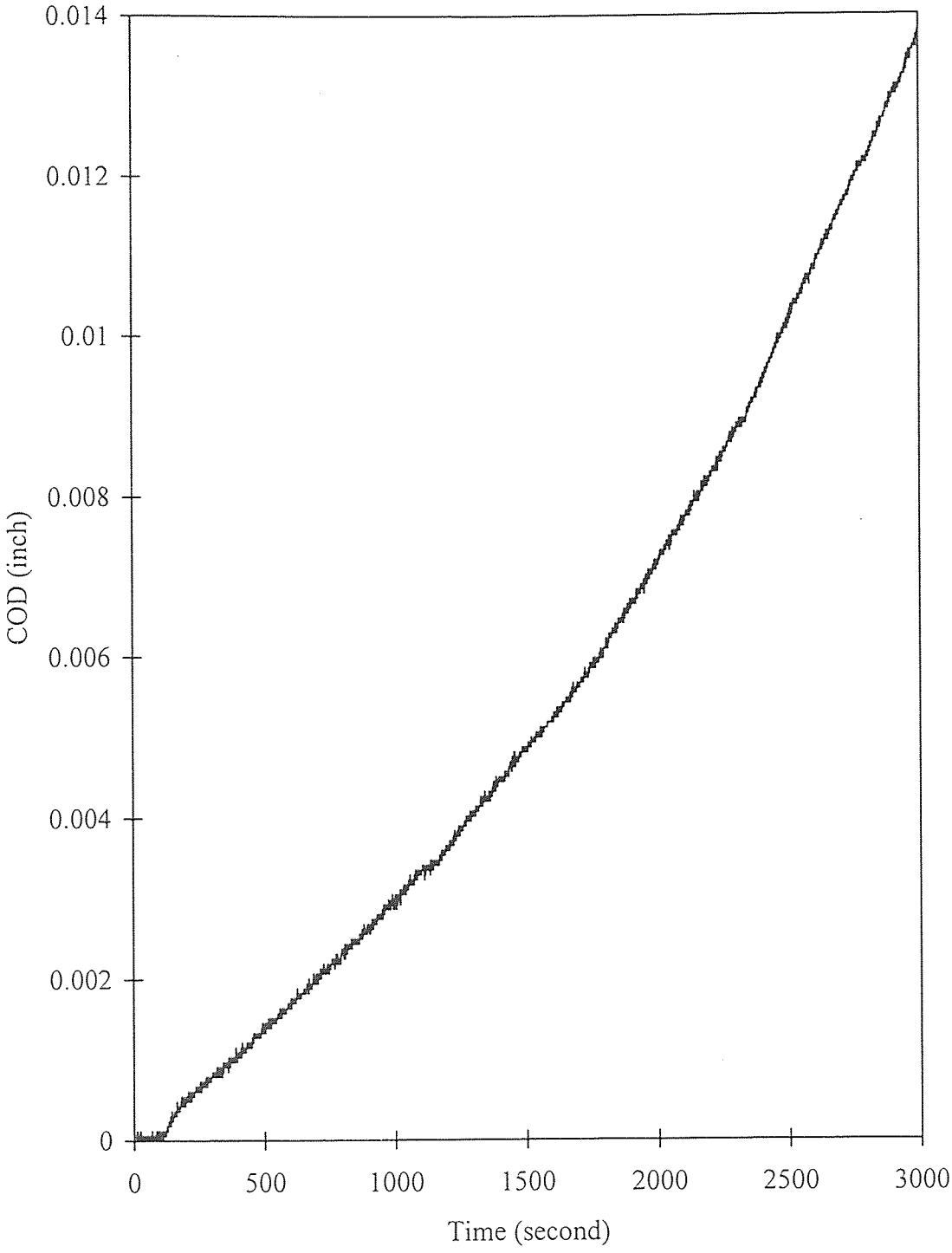


**Figure 4.12** Time vs. COD for n=7.

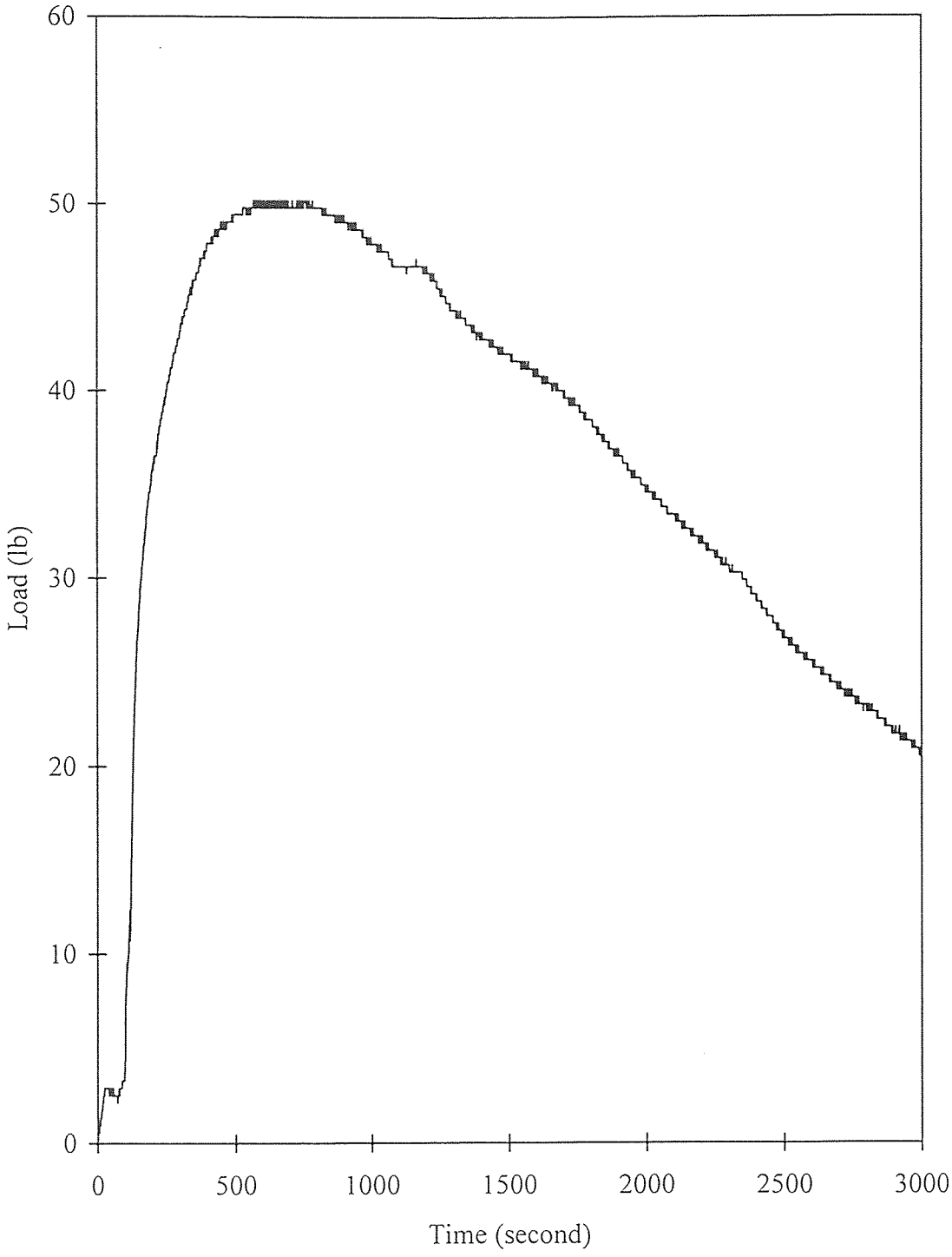


**Figure 4.13** Time vs. load for n=7.

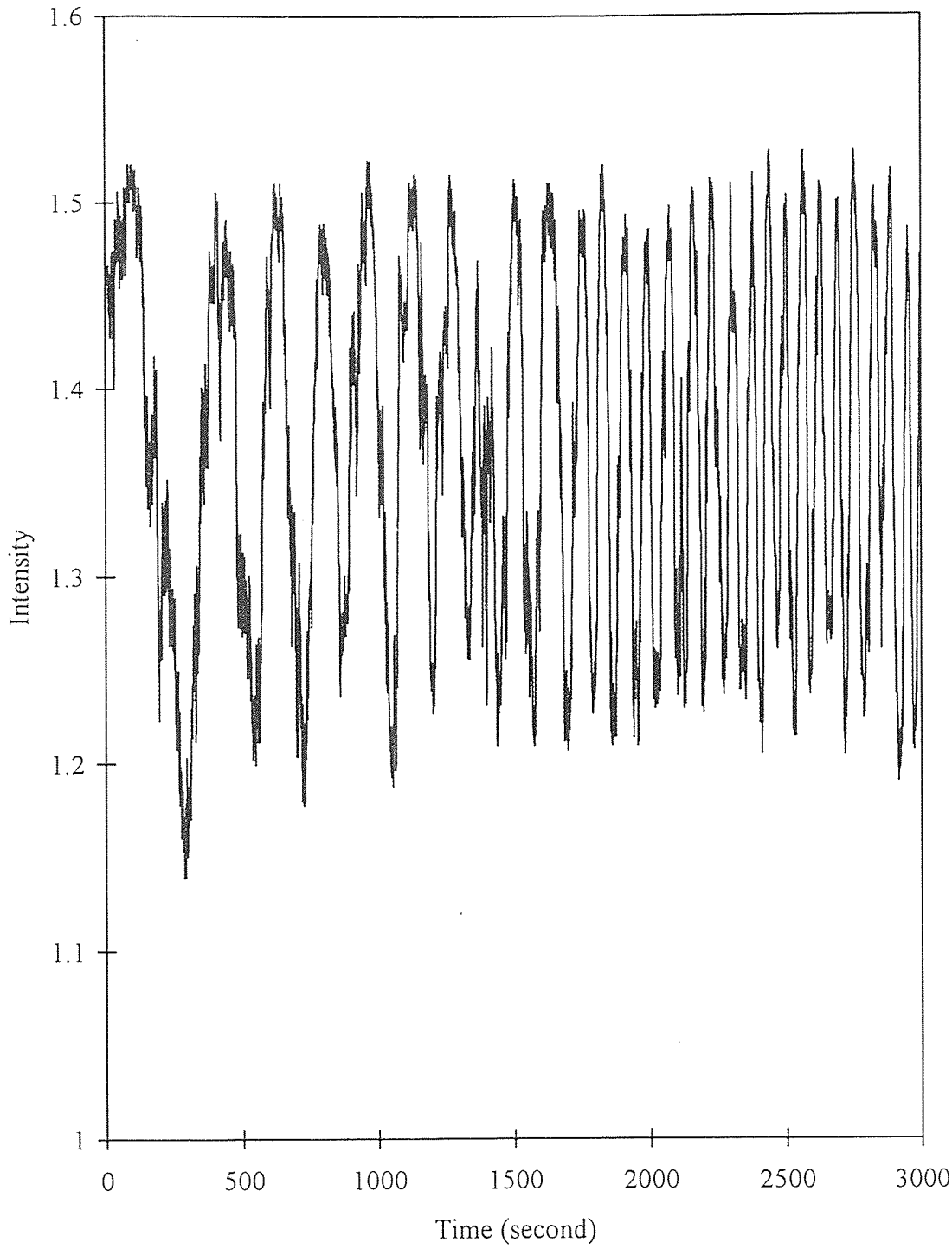


**Figure 4.14** Time vs. intensity for n=7.

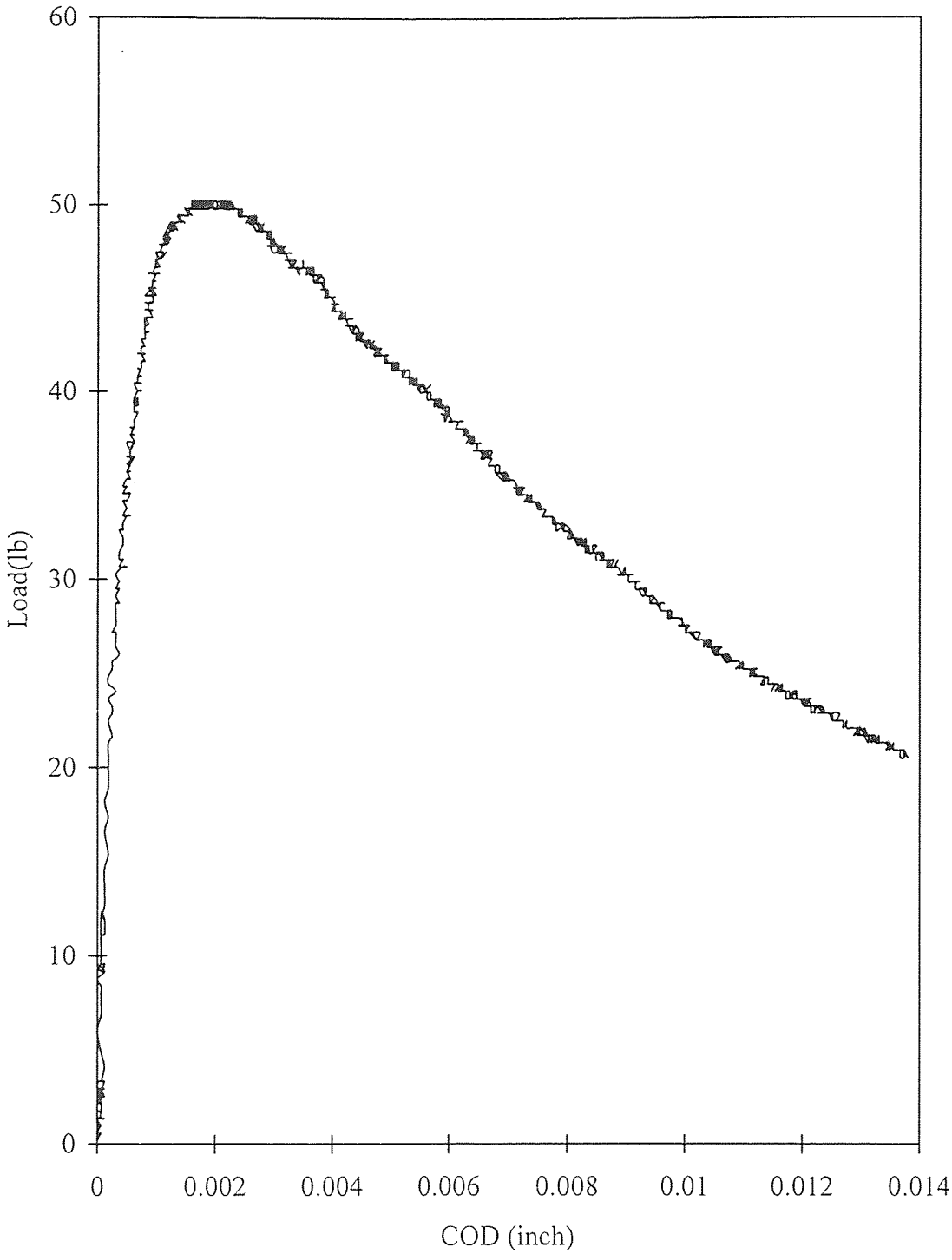


**Figure 4.15** COD vs. load for n=7.

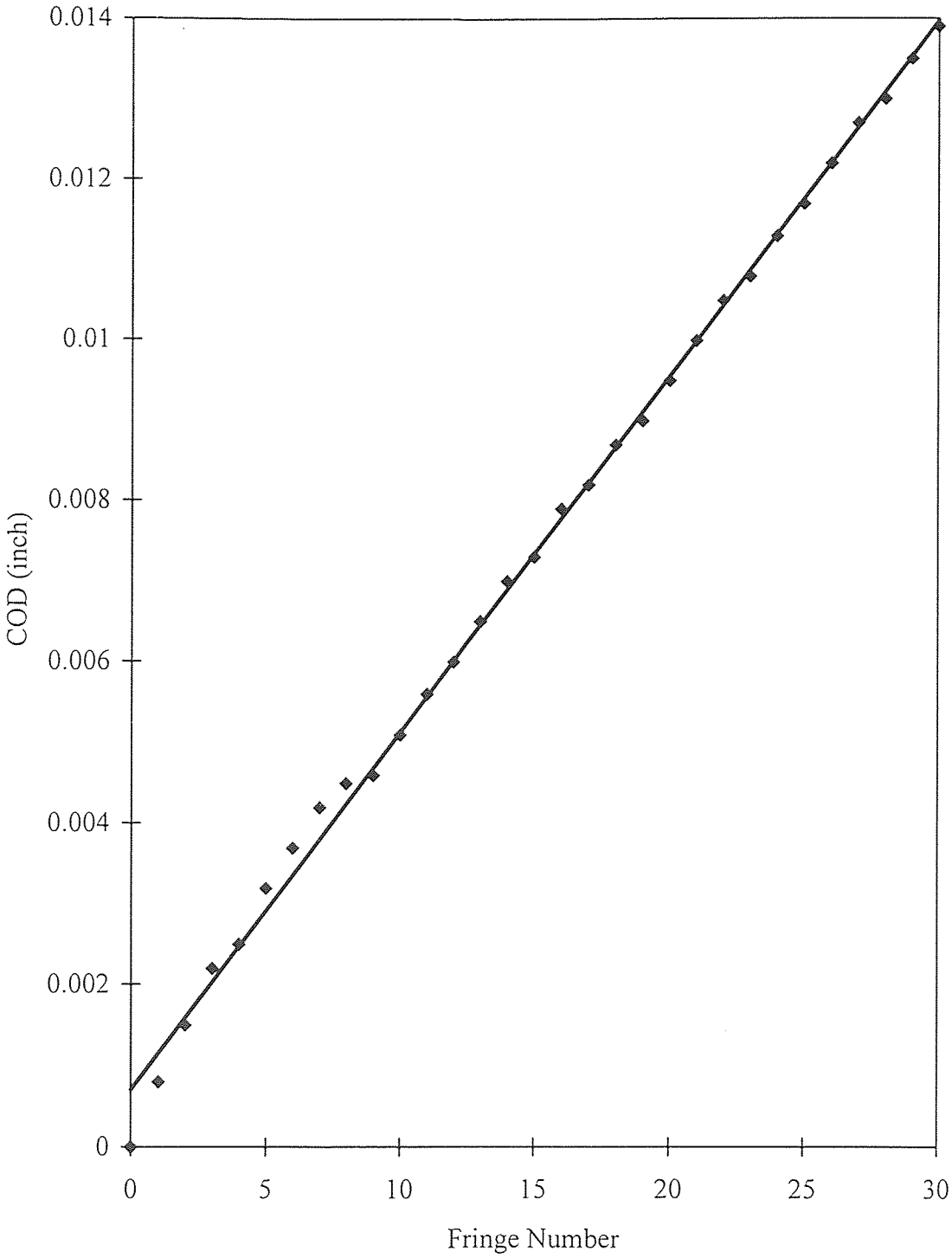


**Figure 4.16** Fringe number vs. COD for n=7.

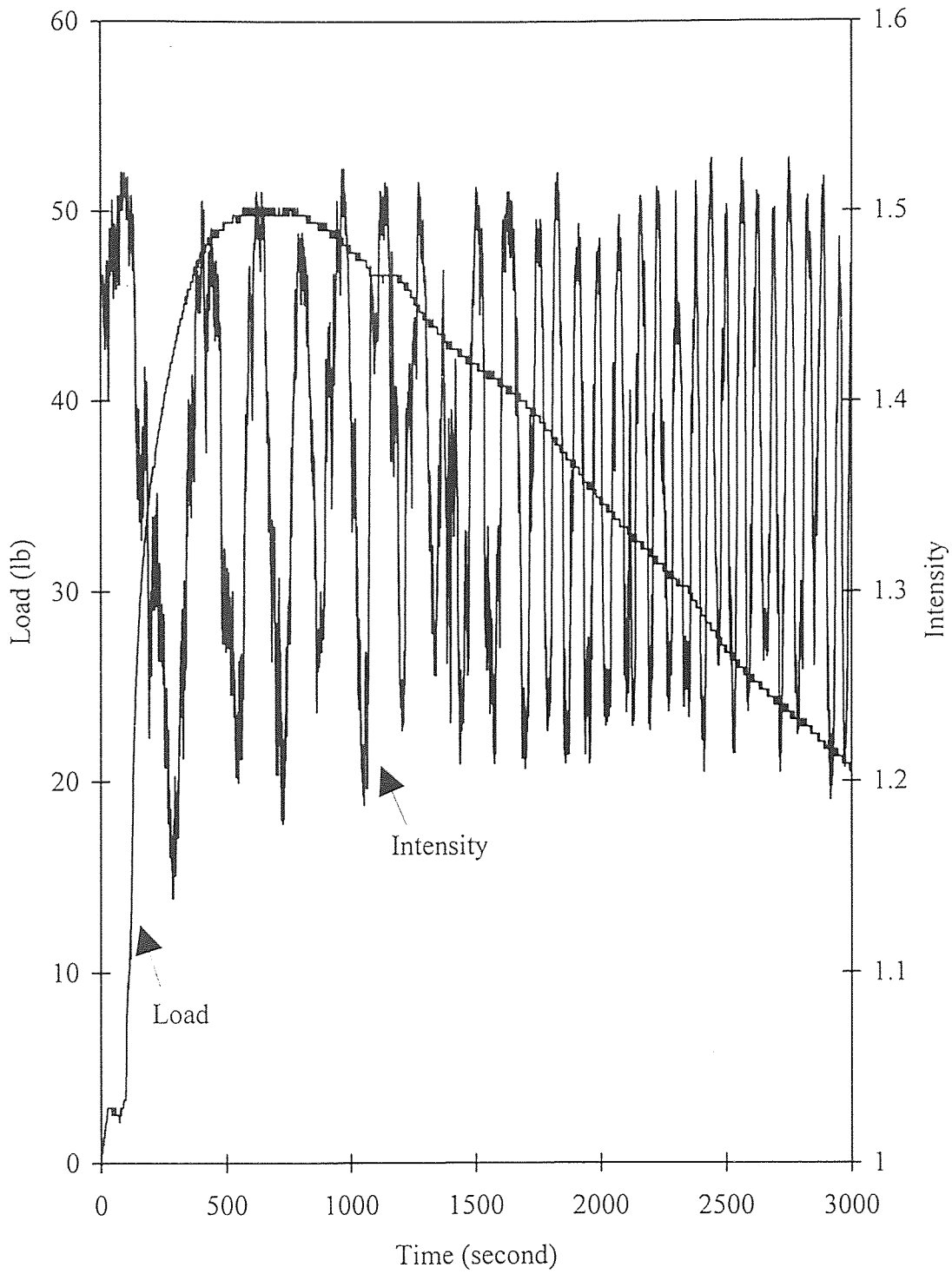


**Figure 4.17** Load vs. CTOD(fringe) data for a beam test.

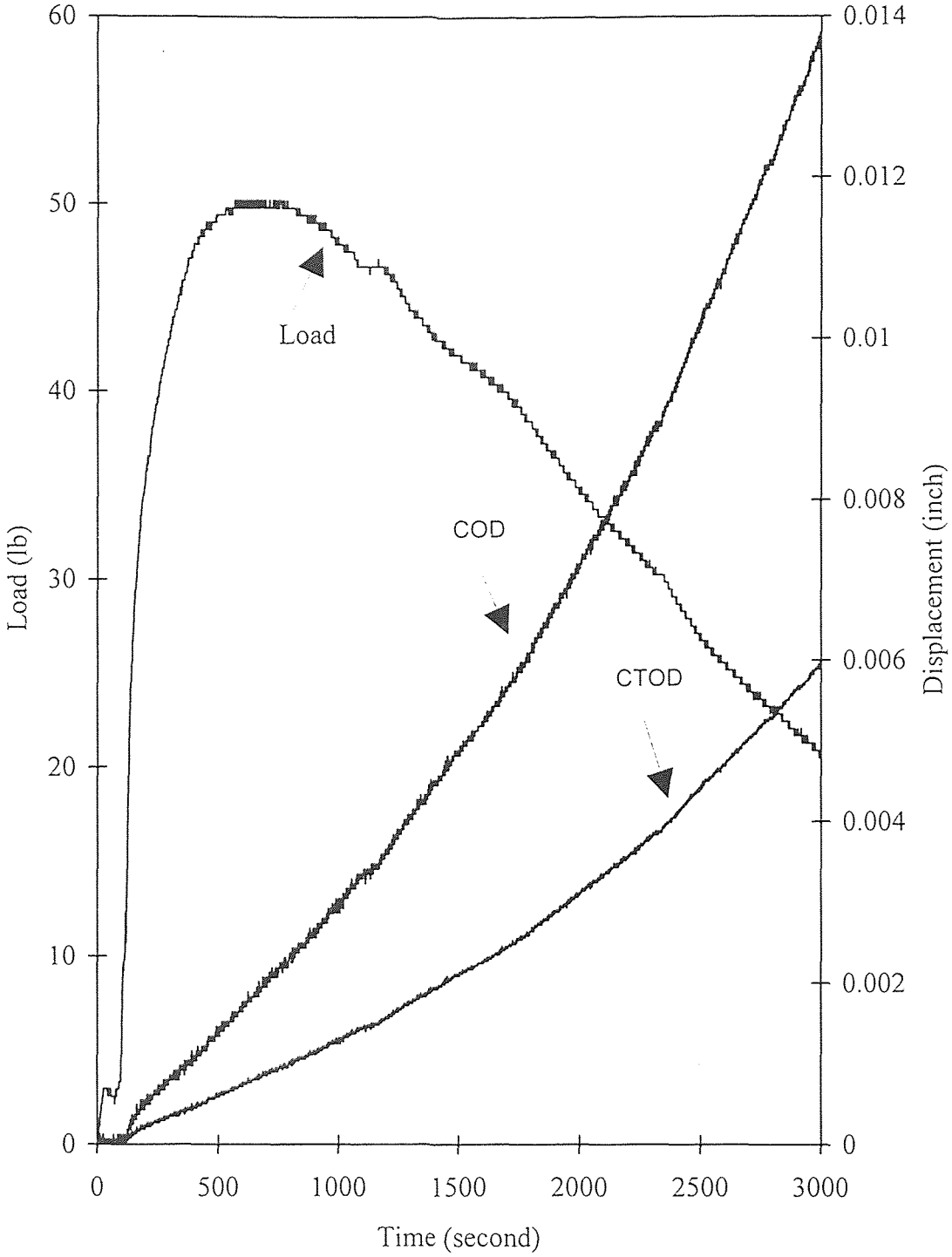


**Figure 4.18** Load, COD, and CTOD data acquired from a beam test.

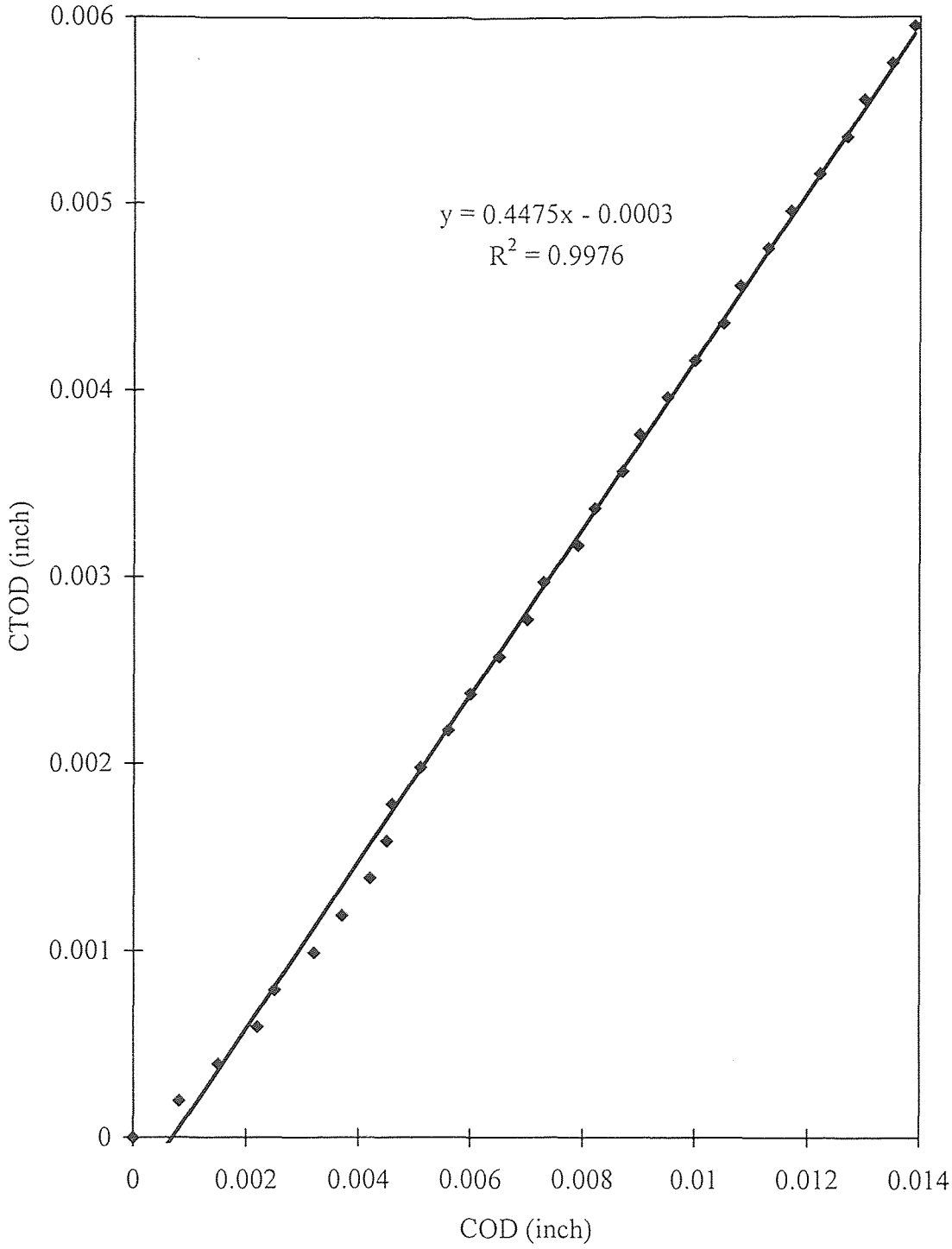


**Figure 4.19** Linear relationship between CTOD and COD.

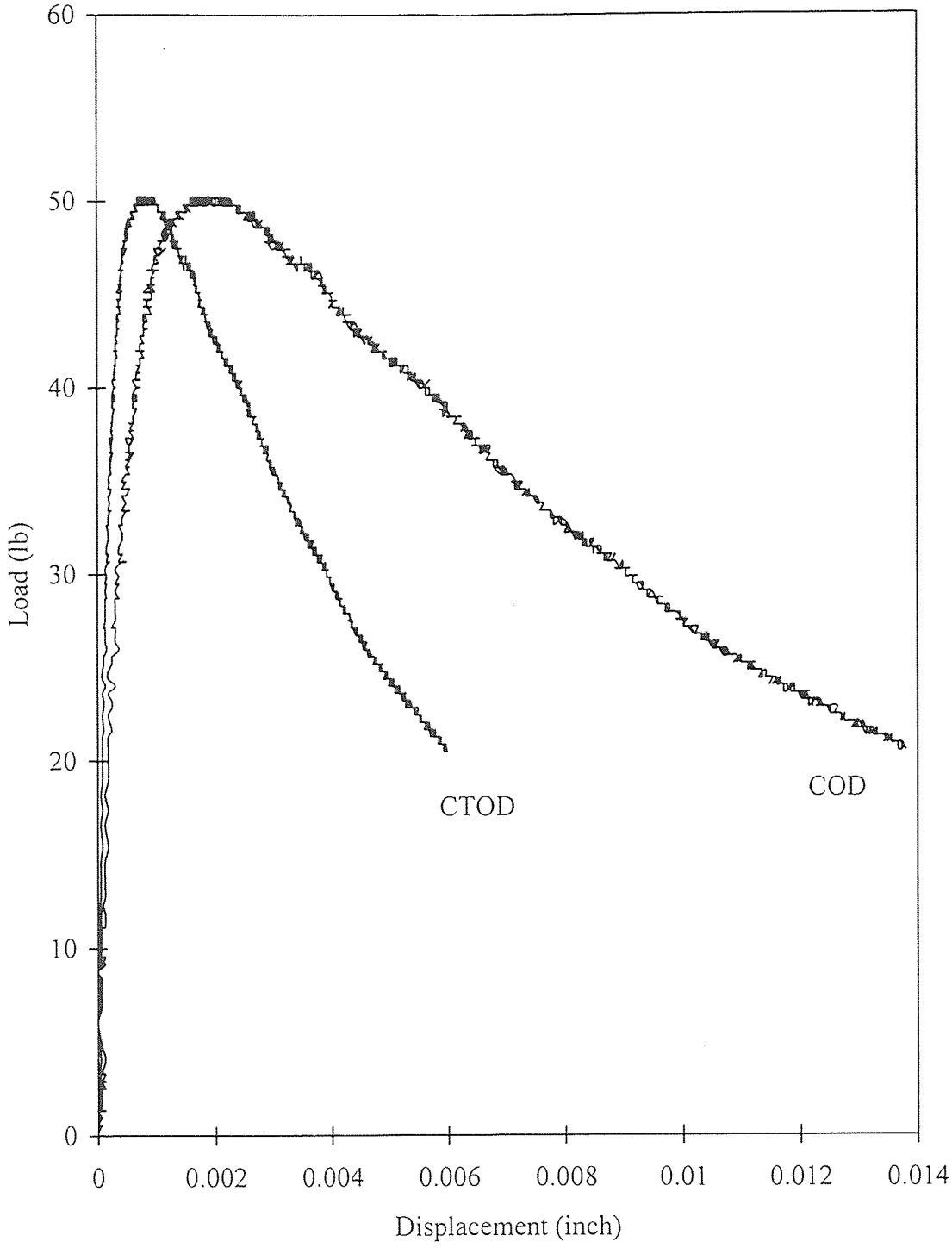


**Figure 4.20** COD and CTOD vs. load.

## REFERENCES


1. Jeng, Y. S., Shah, S. P., "Nonlinear Fracture Parameters for Cement Based Composites:Theory and Experiments," in *Applications of Fracture Mechanics to Cementitious Composites*, Martinus Nijhoff Publishers, Dordrecht, Netherlands, pp. 319-315, 1985.

2. Ansari, F., "Mechanism of Microcrack Formation in Concrete," *ACI Materials Journal*, Title no. 86-M41, Sep.-Oct. 1989, pp. 459-464.

3. Ansari, F., "Stress Strain Response of Microcracked Concrete in Direct Tension, *ACI Materials Journal*, Title no. 84-M42, Nov.-Dec. 1987, pp. 481-490.

4. Ansari, F and Sture, S., *Nondestructive Testing of Concrete Elements and Structures*, American Society of Civil Engineers, New York, NY, 1992.

5. Ansari, F, *Application of Fiber Optic Sensors in Engineering Mechanics*, American Society of Civil Engineers, New York, NY, 1993.

6. Rossi, P., and LeMaou, F., "New method for detecting cracks in concrete using fibre optics", *Materials and Structures, Research and Testing* (RILEM), vol. 22 No. 132, Nov. 1989, pp. 437-442.

7. Nanni, A., Yang, C. C., and Pan, K., "Fiber-Optic Sensors for Concrete Strain/Stress Measurement", *ACI Materials Journal*, Vol. 88, No. 3, May-June, pp.257-264, 1991.

8. Culshaw, B., Gardiner, P.T., and McDonach, A., in *Proceedings of First European Conference on Smart Structures and Materials*, Glasgow, Scotland, 1992.

9. McDonach, A., Gardiner, P. T., McEwen, R. S., and Culshaw, B., in *Proceedings of Second European Conference on Smart Structures and Materials*, Glasgow, Scotland, 1994.

10. Rashleigh, S. C., "Polarimetric sensors: exploiting the axial stress in high birefringence fibers", in *Proceedings of First International Conference on Optical Fiber Sensors*, London, England, pp. 210-213, 1983.

11. Durelli, A. J. and Riley W. F., *Introduction to Photomechanics*, Prentice Hall, Englewood Cliffs, NJ, 1965.

12. Ansari, F. and Wang, J., "Rate sensitivity of high birefringent fiber optic sensors under large dynamic loads", Journal of Lightwave Technology, vol. 13, no. 10, pp.1992-1997 1995.

13. Jackson, D. A., "Monomode optical fiber interferometers for precision measurement" *Journal of Physics*, vol. 18 pp. 981-1001, 1985.